IEEE Access
Multidisciplinary | Rapid Review | Open Access Journal

Received November 21, 2019, accepted December 27, 2019, date of publication January 9, 2020, date of current version January 17, 2020.

Digital Object Identifier 10.1109/ACCESS.2020.2965192

FPMIMO: A General MIMO Structure With Overlapping Subarrays for Various Radar Applications

SYAHFRIZAL TAHCFULLOH[1,2], (Student Member, IEEE), AND GAMANTYO HENDRANTORO[1], (Senior Member, IEEE)

[1]Department of Electrical Engineering, Institut Teknologi Sepuluh Nopember, Surabaya 60111, Indonesia
[2]Department of Electrical Engineering, Universitas Borneo Tarakan, Tarakan 77123, Indonesia

Corresponding author: Syahfrizal Tahcfulloh (syahfrizal15@mhs.ee.its.ac.id)

This work was supported by the Indonesian Ministry of Research, Technology, and Higher Education through the 2015-2018 BPPDN Scholarship No. 028872/IT2/HK.00.00/2015 and the 2017 PKPI Scholarship No. 1469/D3/PG/2017.

ABSTRACT Unlike the phased array (PA) radar that achieves array gain in proportion to the number of elements, the MIMO radar provides improvement to parameter estimation, target detection, and so on. Recently, the combination of the PA and MIMO concepts into the Phased MIMO (PMIMO) radar was proposed with overlapping non-coherent subarrays at the transmitter and an array with non-coherent elements at the receiver that proved to outperform the more conventional radars. This paper examines the parameter identifiability, i.e., the maximum number of detectable targets uniquely identified and the detection performance, i.e., the probabilities of detection and false alarm, of the Full PMIMO radar (FPMIMO), which is a further generalization of combination of the PA and MIMO concepts that uses overlapping subarrays on both transmit and receive arrays. The maximum number of resolvable targets on the FPMIMO radar is derived by the least squares (LS) method and its performance is subsequently evaluated numerically by considering the magnitude of target reflection coefficient as function of direction angle for comparison against PA, MIMO and PMIMO radars. Similarly, the derivation of expressions for probabilities of detection and false alarm is given. In particular, the numerical evaluation is made on the maximum number of resolvable targets with respect to the impact of the number of subarrays, the total number of elements and the element spacing, while the detection performance is evaluated based on the effect of threshold, SNR, and the number of subarrays. The results demonstrate that, being the more general form of multi-antenna radars, the FPMIMO radar is capable of flexibly trading off the maximum number and the lowest reflection coefficient of identifiable targets, with the PA, MIMO and PMIMO radars being special cases. The desired compromise can be obtained by adjusting the number of subarrays on the transmit and the receive arrays. An example of vehicular radar design that satisfies some mission requirements using the FPMIMO radar concept is also presented.

INDEX TERMS MIMO radar, parameter estimation, phased array radar, probability of detection, target detection.

I. INTRODUCTION

Multi-antenna radar systems have been known and used in various applications since 1930s. The most common type is one with phased array (PA), in which multiple elements are fed with different phases to obtain a high coherent gain at a certain direction [1]–[3]. With this advantage, PA radars have been used for such applications as micro-scale radars for biomedical engineering, macro-scale radars on radio-astronomy, and so on [4], [5]. However, in PA radars the number of detected targets is limited by the angular and range resolution. More recently, the multi-input multi-output (MIMO) radar has become an interesting research subject [6]–[18]. Unlike the PA radar, the MIMO radar utilizes many antennas that transmit orthogonal signals to obtain the signal reflected from the target at the receiver, a scheme known as waveform diversity [9]. Consequently, MIMO radars have been successfully applied for radar imaging,

The associate editor coordinating the review of this manuscript and approving it for publication was Dimitris E. Anagnostou.

sonar, aerospace remote sensing, and so on [6]–[8]. However, the MIMO radar, albeit superior in waveform diversity, is weak in directional gain [11].

The problems inherent in the PA and MIMO radars are partially solved by the Phased MIMO radar approach (PMIMO), which exploits the main advantage of the PA radar, i.e., the coherent gain, and that of the MIMO radar, i.e., the diversity gain. This is achieved by forming overlapping non-coherent subarrays (NCS) in the transmit (Tx) array and non-coherent array (NC) at the receive (Rx) array, thereby forming a MIMO structure with the overlapping subarrays replacing single elements at the transmitter [22]–[28]. The purpose of the subarray as an element in the PMIMO radar is to overcome the weakness of the element beam in the MIMO radar that has low directivity, the latter resulting in smaller maximum target range, larger minimum reflection coefficient and susceptibility against interference effects. Hence, the PMIMO radar is designed to operate as a MIMO system with limited space volumes or, equivalently, higher coherent gain at certain directions. The overlapped subarrays method also has a main advantage in minimizing the sidelobe level [20] and can be implemented with a reduced number of devices such as amplifiers, variable phase shifters, etc. [21]. The PMIMO subarrays also have a very low maximum peak sidelobe level (MPSLL) [22]. Another version of the PMIMO radar that employs a receiving all-coherent array (AC) has been investigated in [29].

In the PMIMO radar, transmit subarrays emit orthogonal waveforms associated with matched filters (MFs) in the receive array so that simultaneous multiple beams can be directed to the same target direction while the received waveforms can be distinguished by the receiver. Unlike the PA radar, the PMIMO radar with transmit subarrays as its ''elements'' has a high directional gain in individual subarrays, which in this case look at the same direction [29].

In the works on the PMIMO radar in [22]–[29], the improvement in radar performance factors such as spatial resolution, parameter identifiability, transmit-receive (T-R) gain, and signal-to-interference-plus-noise power ratio (SINR) has been reported. The results of investigations in [29] have demonstrated how the simultaneous application of overlapping subarrays at both the transmitter and the receiver with equal antenna elements on the T-R arrays improves the T-R gain and SINR higher than the PMIMO radar performance observed in [22]–[28]. With respect to the maximum number of detected targets on the PMIMO radar, echoes arriving at the Rx array through beams leading to different targets can be identified through the use of orthogonal waveforms on the Tx arrays and MFs in the Rx arrays [30].

A more general form of array radar systems combining the PA and MIMO concepts has been presented by the authors in [31] by the name of Full Phased MIMO (FPMIMO). The FPMIMO radar also serves as a general architecture for multi-antenna radars that employ overlapped subarrays, which also encompass the class of PMIMO radars [31]. Generally in the FPMIMO system employing K transmit antennas arranged into M overlapped subarrays and L receive antennas with N subarrays, the Tx and Rx may cover either the whole $\mathbb{C}^K$ and $\mathbb{C}^L$ complex space, respectively, or only some subspace of them, i.e., $\mathbb{C}^M$ and $\mathbb{C}^N$, respectively. The subarrays in Rx array are also useful to increase the coherent gain even further relative to the MIMO array. The combination of coherent gain and diversity gain in the Tx-Rx array is expected to produce a high T-R gain and SINR, which are proportional to the enhancement of the maximum number of detected targets. While the concept and performance of FPMIMO radars have been reported by the authors in [31], this paper sets the focus on the radar parameter identifiability and the detection performance.

This paper also expands the study reported in [13], i.e. the maximum number of detectable targets especially for MIMO radars, and the investigation in [15] especially for MIMO radars with non-overlapping subarrays. The formulation on the maximum number of detectable targets on the FPMIMO radar has been derived into a generalized expression of subarrayed MIMO radar by using the least squares (LS) method [13]. While LS is only one of many estimators available, since our paper focuses on the structure of the systems and signals on the radar array and in order to facilitate comparison with MIMO radar results in [13], we use LS in our treatment and leave the use of other estimators for others studies. In addition, expressions for the magnitude of complex amplitude of the target echo from any direction are given for various FPMIMO configurations. Such performance indicators as the maximum number of resolvable targets and probability of detection are studied numerically, especially with respect to the number of subarrays, the total number of elements and the element spacing. The results show the capability of FPMIMO radars in trading off the number of detectable targets and the maximum range or minimum reflection coefficient of the target.

The evaluation on the detection performance in terms of the probability of detection and the probability of false alarm reported herein is an extension of study by [32]. These parameters are evaluated based on several aspects such as the effect of threshold value, SNR, and the number of subarrays in Tx and Rx. Numerical results show the potential of the FPMIMO radar, which exhibits high flexibility.

A holistic consideration on all performance indicators shows that the FPMIMO systems are a generic form of the combination of PA and MIMO where trade off can be made between the parameter identifiability due to waveform diversity and the maximum range due to coherent gain of the subarrays. With the availability of software-defined radar (SDR) technology, such trade-off can be done flexibly depending on given application requirements. In [31], an example of FPMIMO application for bird radar systems has been given. Herein we show another example of the FPMIMO application, which is a vehicular radar.

Generally, in FPMIMO systems, the Tx and Rx may cover either the whole transmit and receive spaces or only some subspace of each of them, depending on the number of

programmed subarrays. Hence, our paper can also be seen as a review of multi-antenna radar techniques that combine the PA and MIMO structures by making use of overlapped subarrays. Aside from that, the main contributions of this paper, which have not been reported before, including in [31], are summarized below:

1) The formulation and the evaluation for the parameter identifiability in the PA, the PMIMO, and the FPMIMO radars to determine the maximum number of detectable targets and the number of elements in a virtual array.
2) The expression and the evaluation of the probability of detection, the probability of miss detection, and the probability of false alarm for the PMIMO and the FPMIMO radars in determining the detection performance.
3) While [31] compares different cases of FPMIMO in terms of T-R gain, SINR, and maximum target range, this paper describes a more complete view of the flexible subarrayed MIMO radar system concept as the generic form of multiple-antenna radar structures that allows trade-off between different performance criteria, consisting of those mentioned in point 1) and 2) as well as those reported in [31].

Following this section, Section II reviews the multi-antenna radar system and signal model, Section III starts with a review of the parameter identifiability for the MIMO radar system and proceeds with the extension of the MIMO case to the more general case of FPMIMO radar and its numerical evaluation. Section IV begins with a review of the detection performance for the PA and MIMO radars and proceeds to discuss the extension of this performance for the FPMIMO radar and its numerical evalution for various parameter values. Section V covers the considerations for implementation and applications. The conclusion is provided in Section VI.

II. MULTI-ANTENNA RADAR SYSTEM AND SIGNAL MODEL

A. SYSTEM MODEL

Fig. 1 presents several examples of configurations in the Tx and Rx arrays for multiple-antenna radar systems. In Fig. 1a, the PA radar consists of the transmitter of a single AC waveform with a high coherent gain while the L elements in the Rx array operate as independent receivers (NC). Hence, it is capable of multi-target detection, although the detected targets are limited because the size of its virtual array (VA) is L. In Fig. 1b, the MIMO radar transmitting K waveforms (NC) that are orthogonal to each other provides the waveform diversity, while the L elements in the Rx side operate as independent receivers (NC) making it suitable for multi-target detection because the VA size is KL. A more specific explanation about the VA is given in part A of Section III.

The comparison of configurations of Tx and Rx between the PMIMO radar, i.e., an FPMIMO radar with $1 \leq M \leq K$ Tx overlapped subarrays and $N = L$ Rx subarrays, and a generic FPMIMO radar using $1 \leq M \leq K$ Tx subarrays and $1 \leq N \leq L$ Rx subarrays are illustrated in Figs. 1c and 1d. On the PMIMO radar, M overlapped subarrays (NCS) in the Tx transmit orthogonal waveforms that compromise between the main advantages of the PA radar (i.e., the directional gain) and the MIMO (i.e., the waveform diversity), while the

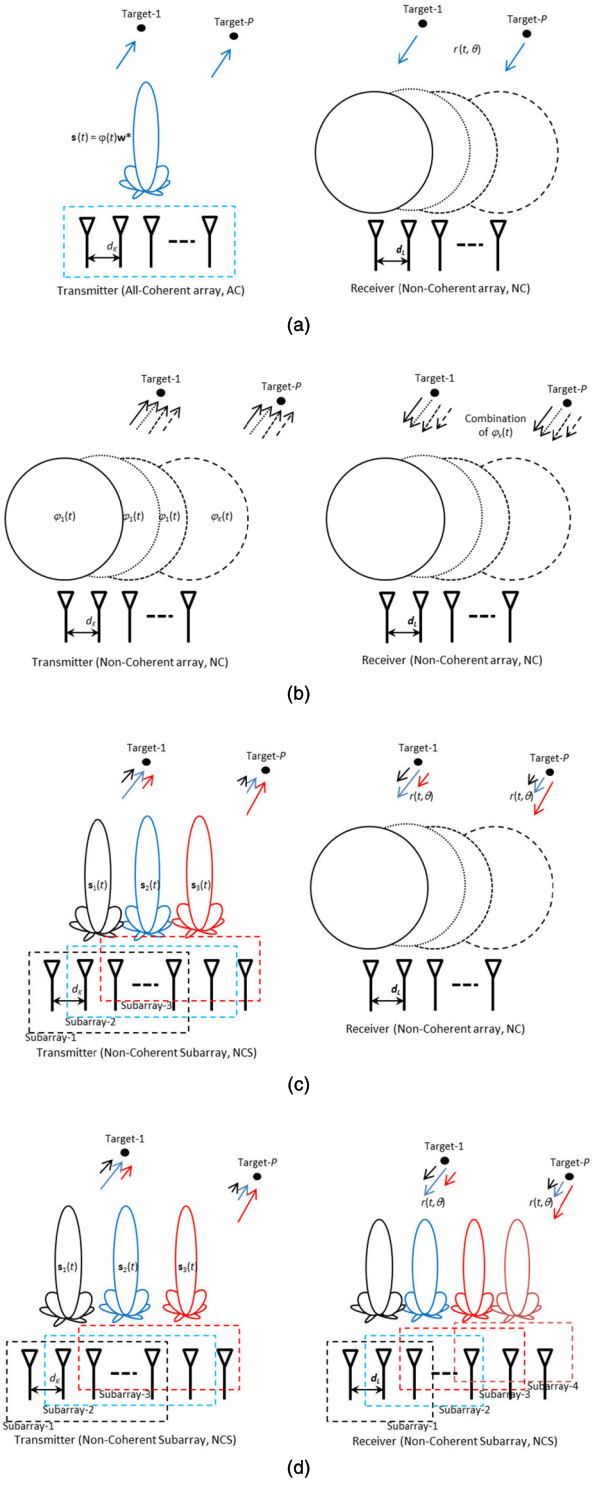

FIGURE 1. Illustrations of FPMIMO arrays on radars: (a) the PA ($M = 1$, $N = L$), (b) the MIMO ($M = K$, $N = L$), (c) the PMIMO ($1 \leq M \leq K$, $N = L$), and (d) another form of FPMIMO ($1 \leq M \leq K$, $1 \leq N \leq L$).

L elements in the Rx operate as NC receivers so that they can detect multiple targets because its VA size is ML, $1 \leq M \leq K$, as presented in Fig. 1c. On the other hand, the FPMIMO radar in Fig. 1d has M NCS on the Tx array and N NCS on Rx so that it simultaneously compromises both the gain at Tx and Rx and the multi-target detection capability. The VA for the FPMIMO radar is MN.

B. SIGNAL MODEL

Suppose a radar system with co-located uniform linear arrays (ULAs) has K antennas on the Tx array and L antennas on the Rx array as in Fig. 1d. The spacing between antenna elements in the Tx and Rx arrays are d_K and d_L, respectively. The transmitted signal is assumed to be narrowband and its propagation is nondispersive. The Tx and Rx arrays have been partitioned into M and N overlapping subarrays, respectively. The number of antenna elements in each subarray is $K_M = K - M+1$ for the Tx array and $L_N = L - N+1$ for the Rx array. Each subarray acts as a PA, so each one forms a beam that leads in a certain direction. A beamforming weight vector is designed to maximize the coherent processing gain across all subarrays on both sides. The block diagram of the FPMIMO radar system is given in [31, Fig. 2].

Subarrays on the Tx array emit unique orthogonal waveforms simultaneously. The m-th subarray on the Tx array emits the signal $\varphi_m(t)$ where the signal is orthogonal to those from the other subarrays. Assume that the m-th subarray consists of $K - M+1 < K$ elements of the Tx array, then the baseband signal model for the m-th subarray with unit energy can be expressed by the signal vector $\psi(t) = [\varphi_1(t)\varphi_2(t) \ldots \varphi_M(t)]^T$.

The K-element complex envelope vector of the transmitted baseband signal on the m-th subarray is

$$\mathbf{s}_m(t) = \sqrt{K/M}\varphi_m(t)\mathbf{w}_m^* \quad m = 1, 2, \ldots, M \tag{1}$$

where K/M is the normalizing coefficient of power, which ensures that the energy sent by the FPMIMO radar in a radar pulse is equal to K, and $\mathbf{w}_m$ is the unit-norm K-element complex weight vector for the m-th transmit subarray with $K - M+1$ beamforming weights corresponding to the active antenna elements of the m-th subarray. Hence, the number of non-zero weights in $\mathbf{w}_m$ is equal to $K - M+1$, while the other $M+1$ are zero. Accordingly, the $M \times K$ matrix of the subarray envelopes of the Tx array, i.e. $\mathbf{S}(t) = [\mathbf{s}_1(t)\ \mathbf{s}_2(t) \ldots \mathbf{s}_M(t)]^T$, must satisfy the following orthogonal requirement

$$\int_{T_P} \mathbf{S}(t)\mathbf{S}^H(t)dt = \mathbf{I}_{M\times M} \tag{2}$$

where T_p is the pulse repetition interval (PRI).

If the total energy emitted by the K-element transmit array in one PRI is K, then the energy of signal $\mathbf{s}_m(t)$ on the m-th subarray in one PRI is

$$E_M = \int_{T_P} \mathbf{s}_m^H(t)\mathbf{s}_m(t)dt = K/M \tag{3}$$

Hence, the total energy of M subarrays in one PRI equals K and the energy per element in a subarray is $K/(M \times (K - M+1))$.

The signal reflected by a target located at θ in the far field with reflection coefficient $\sigma(\theta)$ is expressed as

$$r(t, \theta) = \sqrt{K/M}\sigma(\theta) \sum_{m=1}^{M} \mathbf{w}_m^H \mathbf{a}_m(\theta) e^{-j2\pi f \tau_m(\theta)} \varphi_m(t) \tag{4}$$

where $\mathbf{a}_m(\theta)$ denotes a K-element transmit steering vector on the m-th subarray, $\tau_m(\theta)$ the relative delay of the first element of the m-th subarray to the first element of the first subarray with $\tau_m(\theta) = md_K \sin(\theta)/c$, where c is the speed of light.

Define the M-element transmit coherent vector $\mathbf{c}(\theta)$ and the transmit diversity vector $\mathbf{d}(\theta)$ as

$$\mathbf{c}(\theta) = \begin{bmatrix} \mathbf{w}_1^H \mathbf{a}_1(\theta) & \mathbf{w}_2^H \mathbf{a}_2(\theta) & \ldots & \mathbf{w}_M^H \mathbf{a}_M(\theta) \end{bmatrix}^T \tag{5}$$

$$\mathbf{d}(\theta) = \begin{bmatrix} e^{-j2\pi f \tau_1(\theta)} & e^{-j2\pi f \tau_2(\theta)} & \ldots & e^{-j2\pi f \tau_M(\theta)} \end{bmatrix}^T \tag{6}$$

then (4) can be simplified into

$$r(t, \theta) = \sqrt{K/M}\sigma(\theta)(\mathbf{c}(\theta) \circ \mathbf{d}(\theta))^T \boldsymbol{\psi}(t) \tag{7}$$

where $\circ$ denotes the Hadamard product.

Assume that there are P targets in the directions of $\{\theta_p\}$ with $p = 1, \ldots, P$, then the N-element received complex vector is

$$\mathbf{y}_{\text{FPMIMO}}(t) = \sum_{p=1}^{P} r(t, \theta_p)(\mathbf{g}(\theta_p) \circ \mathbf{h}(\theta_p)) + \mathbf{n}(t) \tag{8}$$

or

$$\mathbf{y}_{\text{FPMIMO}}(t) = \sqrt{K/M} \sum_{p=1}^{P} \sigma_p(\theta_p)[\mathbf{g}(\theta_p) \circ \mathbf{h}(\theta_p)] \cdot [\mathbf{c}(\theta_p) \circ \mathbf{d}(\theta_p)]^T \boldsymbol{\psi}(t) + \mathbf{n}(t) \tag{9}$$

with

$$\mathbf{g}(\theta) = \begin{bmatrix} \mathbf{v}_1^H \mathbf{b}_1(\theta) & \mathbf{v}_2^H \mathbf{b}_2(\theta) & \ldots & \mathbf{v}_N^H \mathbf{b}_N(\theta) \end{bmatrix}^T \tag{10}$$

$$\mathbf{h}(\theta) = \begin{bmatrix} e^{-j2\pi f \tau_1(\theta)} & e^{-j2\pi f \tau_2(\theta)} & \ldots & e^{-j2\pi f \tau_N(\theta)} \end{bmatrix}^T \tag{11}$$

where $\mathbf{b}_n(\theta)$ denotes the L-element receive steering vector on the n-th subarray, $\mathbf{v}_n$ the L-element unit-norm complex weight vector of the n-th subarray on the Rx array with the same definition as $\mathbf{w}_m$, $\mathbf{g}(\theta)$ the N-element receive coherent vector, $\mathbf{h}(\theta)$ the N-element receive diversity vector, and $\mathbf{n}(t)$ the N-element vector for white zero-mean noise and interference. It is worth noting that, unlike (8), the received vector in (11) of [31] assumes a single target with P interferences.

Furthermore, by using matched filter banks to separate terms containing orthogonal waveforms $\{\varphi_m(t)\}$, a MN-element vector is obtained

$$\mathbf{u} = \begin{bmatrix} \mathbf{y}_1^T & \mathbf{y}_2^T & \ldots & \mathbf{y}_M^T \end{bmatrix}^T = \sqrt{K/M} \sum_{p=1}^{P} \sigma_p(\theta_p)\mathbf{e}(\theta_p) + \mathbf{n} \tag{12}$$

where the time variable t is hidden and

$$y_m = \sqrt{K/M}\sum_{p=1}^{P}\sigma_p(\theta_p)e(\theta_p) + \mathbf{n},$$

with the MN-element T-R steering vector

$$\mathbf{e}(\theta) = (\mathbf{c}(\theta)\circ\mathbf{d}(\theta))\otimes(\mathbf{g}(\theta)\circ\mathbf{h}(\theta)) \tag{13}$$

Notation $\otimes$ denotes the Kronecker product operator, $\sigma_p(\theta_p)$ the radar reflection coefficient of the p-th target and $\mathbf{n}$ the MN-element noise vector including the interference at the receiver. For the p-th target, $\sigma_p(\theta_p)$ is independent from other targets and is a white Gaussian process with zero mean and variance σ_p^2 or $\sigma_p(\theta_p) \sim \mathcal{CN}(0, \sigma_p^2)$ [13]. It is assumed that neither noise nor interference correlates with the transmitted signal $\varphi_m(t)$.

III. PARAMETER IDENTIFIABILITY

A. VIRTUAL ARRAY

The target detection, the angular accuracy, and the maximum number of detectable targets are strongly dictated by the VA dimension in MIMO radar systems as reported by [17]. The relationship between the VA size and the maximum number of detectable targets for the MIMO and the PA radar has been described by [13]. In a MIMO radar, in which K elements in the Tx array transmit orthogonal waveforms and L elements in the Rx array receive echo signals from targets operating independently, the VA dimension is expressed as [13], [17]

$$\mathcal{N}_{\text{MIMO}} \in [K + L - 1, KL] \tag{14}$$

where $\mathcal{N}_{\text{MIMO}}$ is the integer number of virtual elements. The interval in (14) can be interpreted as that of the number of virtual elements from VA with the lower limit $\mathcal{N}_{\text{MIMO}} = (K+L-1)$ occurring when the element spacing in Tx and Rx is $d_K = d_L = d$ and the upper limit $\mathcal{N}_{\text{MIMO}} = KL$ is achieved when $d_K = Ld_L$ and $d_L = d$. Generally, $d = 0.5\lambda$ is chosen for element spacing to minimize the mutual coupling effect and to avoid grating lobes in phased arrays [13].

For a PA radar that transmits a coherent waveform having an echo signal received by L independent elements in Rx, the number of virtual elements in the VA is [13], [17]

$$\mathcal{N}_{\text{PA}} = L \tag{15}$$

We can extend the above results to the generic FPMIMO and the PMIMO case as follows. For a FPMIMO radar with a Tx array that uses M overlapped subarrays to radiate M orthogonal waveforms and a Rx array consisting of N overlapped subarrays as independent receive elements, the number of virtual elements in the VA is

$$\mathcal{N}_{\text{FPMIMO}} \in [M + N - 1, MN] \tag{16}$$

As a special case of the FPMIMO radar, the PMIMO radar only uses M overlapped subarrays in the Tx array that transmit M orthogonal waveforms. Echo signals from the targets are received by L elements in the Rx so that the number of virtual elements in the VA is

$$\mathcal{N}_{\text{PMIMO}} \in [M + L - 1, ML] \tag{17}$$

The number of virtual elements in the VA for radars with overlapping subarrays on Tx and/or Rx, referred to herein as the subarrayed MIMO (SMIMO) radars, such as the FPMIMO radar, ranges between two extreme configurations, namely the PA and the MIMO radar. That is, $\mathcal{N}_{\text{PA}} \leq \mathcal{N}_{\text{SMIMO}} \leq \mathcal{N}_{\text{MIMO}}$. This is because the SMIMO radar uses overlapping subarrays, so that the formed waveforms are not perfectly orthogonal and make the number of virtual elements in the VA lower than that of the MIMO radar. However, applying the concept of the FPMIMO radar as a generic form for the MIMO radar is beneficial thanks to its flexibility due to the degrees of freedom (DoF) provided by the numbers M and N of subarrays in the Tx-Rx arrays. In the case of the PMIMO radar, the Rx array is fixed with $N = L$. This implies that the PA, the MIMO, and the PMIMO radar are special conditions of the FPMIMO radar i.e., FPMIMO ($M = 1, N = L$), FPMIMO ($M = K, N = L$), and FPMIMO ($1 \leq M \leq K, N = L$), respectively.

B. REVIEW ON MAXIMUM NUMBER OF DETECTED TARGETS FOR MIMO RADAR

For clarity in discussions that follow, herein we provide a short review of the performance of MIMO radars in the maximum number of detected targets, mostly taken from [13]. Suppose a MIMO radar system with co-located ULAs has K antennas on the Tx array and L antennas on the Rx array. The L-element vector of the received signal with target direction θ_p is [13]

$$\mathbf{y}_{\text{MIMO}}(t) = \sum_{p=1}^{P}\sigma_p(\theta_p)\mathbf{b}(\theta_p)\mathbf{a}^T(\theta_p)\boldsymbol{\psi}(t) + \mathbf{n}(t) \tag{18}$$

where $(\cdot)^T$ denotes the transpose operator, P the number of targets, θ_p the location of the p-th target, $\sigma(\theta)$ the radar reflection coefficient of the target at direction θ, $\mathbf{a}(\theta) = [1 \; e^{-j2\pi d_K \sin(\theta)/\lambda} \; \ldots e^{-j2\pi(K-1)d_K\sin(\theta)/\lambda}]^T$ the K-element transmit steering vector at θ, $\mathbf{b}(\theta) = [1e^{-j2\pi d_L\sin(\theta)/\lambda} \; \ldots e^{-j2\pi(L-1)d_L\sin(\theta)/\lambda}]^T$ the L-element receive steering vector with a definition similar to $\mathbf{a}(\theta)$, d_K and d_L the spacing between antenna elements in the transmit and receive array, respectively, λ the carrier wavelength, $\psi(t) = [\varphi_1(t)\varphi_2(t) \ldots \varphi_K(t)]^T$ a vector of the transmitted baseband signals from the K transmit antennas in discrete time with $t = 1, 2, \ldots, Q$, and $\mathbf{n}(t)$ the L-element vector for noise and interference from targets in other locations uncorrelated with reflections from the P targets.

The spatial spectrum of the target reflection coefficient magnitude obtained by the least squares (LS) method is defined as [13]

$$\hat{\sigma}_{\text{MIMO}}(\theta) = \frac{\sum_{q=1}^{Q}\mathbf{b}^H(\theta)\hat{\mathbf{R}}_{\mathbf{y}\boldsymbol{\psi}}\mathbf{a}^*(\theta)}{\|\mathbf{b}(\theta)\|^2\,\mathbf{a}^T(\theta)\hat{\mathbf{R}}_{\boldsymbol{\psi}\boldsymbol{\psi}}\mathbf{a}^*(\theta)} \tag{19}$$

with

$$\hat{\mathbf{R}}_{\mathbf{y}\boldsymbol{\psi}} = (1/Q)\sum_{q=1}^{Q} \mathbf{y}_{\text{MIMO}}(q)\boldsymbol{\psi}^H(q) \tag{20}$$

$$\hat{\mathbf{R}}_{\boldsymbol{\psi}\boldsymbol{\psi}} = (1/Q)\sum_{q=1}^{Q} \boldsymbol{\psi}(q)\boldsymbol{\psi}^H(q) = \mathbf{I}_{K\times K} \tag{21}$$

where $||\cdot||$ denotes the Euclidean norm, $(\cdot)^H$ the Hermitian transpose operator, $(\cdot)^*$ the complex conjugate operator, $\hat{\sigma}_{\text{MIMO}}(\theta)$ the LS estimation for the radar reflection coefficient or magnitude of the complex amplitude of the target at direction θ, and $q = 1, 2, \ldots, Q$ is the index of data sample. The number of detectable targets can be identified from the peaks of the spatial spectrum.

C. MAXIMUM NUMBER OF DETECTED TARGETS FOR FPMIMO RADAR

The parameters of FPMIMO radar performance such as T-R gain, SINR, and maximum range have been derived, with the PMIMO, the MIMO, and the PA radar as special cases, in [31]. Specifically, the SINR gain on the FPMIMO radar depending on the number N of Rx subarrays is $(N/L)(L - N+1)$ times the SINR obtained by the PMIMO radar, in which $N = L$.

In [13] it is stated that to determine parameter estimates such as the maximum number of detectable targets, the SINR must be infinite so that the noise in the receiver can be ignored and does not correlate with the transmit signal.

As in the derivation of parameter identifiability of MIMO radar in [13], the baseband-equivalent signal is received by the L-element Rx array consisting of N overlapping subarrays for θ_p on the FPMIMO radar as in (9). The parameters to be estimated from $\mathbf{y}_{\text{FPMIMO}}(t)$ are $\{\sigma_p(\theta_p)\}_{p=1}^{P}$ and $\{\theta_p\}_{p=1}^{P}$. Let $\mathbf{n}(t)$ be uncorrelated with $\psi(t)$, then the identifiability property of the first term of (9) is not influenced by the second term.

The identifiability equation for FPMIMO is extended from that of MIMO in [13, Eq. (7)] to include the subarrays and can be given as follows

$$\sum_{p=1}^{P} \breve{\sigma}_p(\breve{\theta}_p)[\mathbf{g}(\breve{\theta}_p)\circ\mathbf{h}(\breve{\theta}_p)][\mathbf{c}(\breve{\theta}_p)\circ\mathbf{d}(\breve{\theta}_p)]^T\boldsymbol{\psi}(t) = \sum_{p=1}^{P} \sigma_p(\theta_p)[\mathbf{g}(\theta_p)\circ\mathbf{h}(\theta_p)][\mathbf{c}(\theta_p)\circ\mathbf{d}(\theta_p)]^T\boldsymbol{\psi}(t) \tag{22}$$

For the existence of parameter identifiability, (22) shall have a unique solution for each of $\breve{\sigma}_p(\breve{\theta}_p) = \sigma_p(\theta_p)$, $\breve{\theta}_p = \theta_p$, $p = 1, 2, \ldots, P$. The assumption is that the M transmitted waveforms are linearly independent from one another, so that the following is satisfied:

$$\text{rank}\left\{\left[\boldsymbol{\psi}(1)\ \ \boldsymbol{\psi}(2)\ \ \ldots\ \ \boldsymbol{\psi}(Q)\right]\right\} = M, \quad Q \geq M \tag{23}$$

Subsequently, (22) can be simplified to

$$\sum_{p=1}^{P} \breve{\sigma}_p(\breve{\theta}_p)[\mathbf{g}(\breve{\theta}_p)\circ\mathbf{h}(\breve{\theta}_p)][\mathbf{c}(\breve{\theta}_p)\circ\mathbf{d}(\breve{\theta}_p)]^T = \sum_{p=1}^{P} \sigma_p(\theta_p)[\mathbf{g}(\theta_p)\circ\mathbf{h}(\theta_p)][\mathbf{c}(\theta_p)\circ\mathbf{d}(\theta_p)]^T \tag{24}$$

or

$$\breve{\mathbf{A}}\breve{\sigma} = \mathbf{A}\sigma \tag{25}$$

where

$$\boldsymbol{\sigma} = \left[\sigma_1(\theta_1)\quad \sigma_2(\theta_2)\quad \ldots\quad \sigma_P(\theta_P)\right]^T \tag{26}$$

$$\breve{\boldsymbol{\sigma}} = \left[\breve{\sigma}_1(\breve{\theta}_1)\quad \breve{\sigma}_2(\breve{\theta}_2)\quad \ldots\quad \breve{\sigma}_P(\breve{\theta}_P)\right]^T \tag{27}$$

$$\boldsymbol{\alpha}_p = [\mathbf{g}(\theta_p)\circ\mathbf{h}(\theta_p)][\mathbf{c}(\theta_p)\circ\mathbf{d}(\theta_p)]^T \tag{28}$$

$$\breve{\boldsymbol{\alpha}}_p = [\mathbf{g}(\breve{\theta}_p)\circ\mathbf{h}(\breve{\theta}_p)][\mathbf{c}(\breve{\theta}_p)\circ\mathbf{d}(\breve{\theta}_p)]^T \tag{29}$$

$$\mathbf{A} = \left[\boldsymbol{\alpha}_1\quad \boldsymbol{\alpha}_2\quad \ldots\quad \boldsymbol{\alpha}_P\right]^T \tag{30}$$

$$\breve{\mathbf{A}} = \left[\breve{\boldsymbol{\alpha}}_1\quad \breve{\boldsymbol{\alpha}}_2\quad \ldots\quad \breve{\boldsymbol{\alpha}}_P\right]^T \tag{31}$$

The maximum number of detectable targets on the FPMIMO radar is derived in analogy to that of the MIMO radar reported in [13, Eq. (22)]. If there are K antennas on the Tx array that form M overlapping subarrays to transmit linear independent waveforms and L antennas on the Rx array that forms N overlapping subarrays with their respective matched filters for the independent waveforms, sufficient and necessary conditions for the identification of FPMIMO radar parameters are

$$P_{max,\text{FPMIMO}} \in \left[\frac{M+N-2}{2}\ ,\ \frac{MN+1}{2}\right) \tag{32}$$

The range of the maximum number of detectable targets from the FPMIMO radar in (32) depends on the number of subarrays in the Tx and Rx arrays (i.e., M and N). Unlike in the MIMO radar [13], the number of antenna elements in the Tx and Rx arrays, K and L, does not directly determine the maximum number of detectable targets on the FPMIMO radar. The number of each of Tx and Rx subarrays formed on a FPMIMO radar ranges in $1 \leq M \leq K$ and $1 \leq N \leq L$, respectively, with the MIMO radar being a special case of FPMIMO radars where $M = K$ and $N = L$. Thus, the actual value of the maximum number of detectable targets achieved by the FPMIMO radar having different subarray configurations is lower than the MIMO radar because $M \leq K$ and $N \leq L$. This is also because when compared to MIMO the use of overlapping subarrays on T-R arrays in the FPMIMO radar has a positive effect on the high directional coherent gain, which is proportional to the high magnitude of complex amplitude (MCA) of detectable target. The simulation results of the FPMIMO radar that have been carried out show that such use of T-R subarrays has the advantage of being able to balance the MCA between two targets, as required by the given application [31].

Based on (32) and following the results in [13], the range of maximum number of detectable targets for the PMIMO radar, where $1 \leq M \leq K$ and $N = L$, can also be derived from the FPMIMO radar. For the PMIMO radar, (32) becomes

$$P_{max,\text{PMIMO}} \in \left[\frac{M+L-2}{2}\ ,\ \frac{ML+1}{2}\right) \tag{33}$$

In (33), the maximum number of detectable targets on the PMIMO radar depends on the number of subarrays on the Tx array side and the number of antenna elements on the Rx array side. The number of each of the Tx and Rx subarrays in PMIMO radar is $1 \leq M \leq K$ and $N = L$, respectively, and hence $P_{max,\text{PMIMO}} \geq P_{max,\text{FPMIMO}}$. This indicates that the use of overlapping subarrays on the Tx array can control the magnitude of complex amplitude of detectable target. The Rx array on the PMIMO radar does not use subarrays, which means a non-coherent array (NC), so that it maximizes the waveform diversity gain to an extent limited by the number of Tx subarrays and Rx antennas. The waveform diversity gain has an impact on the decrease of the MCA but also implies an increasing number of detectable targets.

While (32) and (33) are our own findings, the maximum number of detected targets for PA and MIMO radars as given in [13, Eq. (25) and (22)] can also be obtained from (32), those being special conditions of the FPMIMO radar. Thus, for the FPMIMO radar, the following relationship applies, $P_{max,\text{MIMO}} \geq P_{max,\text{FPMIMO}} \geq P_{max,\text{PA}}$.

D. COMPLEX AMPLITUDE OF TARGET ECHO

It is necessary to estimate $\sigma(\theta)$ for each target direction θ from the received vector $\mathbf{y}_{\text{FPMIMO}}(t)$. The estimate $\hat{\sigma}(\theta)$ of $\sigma(\theta)$ can be used to form spatial spectra, which in turn can be used to estimate locations of all targets by finding distinguishable peaks in it. To obtain the number of detected targets on the MIMO radar, the LS method used in [13]–[15] is used herein against the N-element vector of received signals in (9). The estimate $\hat{\sigma}(\theta)$ can be obtained when both sides of (9) are multiplied from the left by the transpose conjugate of $[\mathbf{g}(\theta_p) \circ \mathbf{h}(\theta_p)]$ as follows:

$$[\mathbf{g}(\theta_p) \circ \mathbf{h}(\theta_p)]^H \mathbf{y}_{\text{FPMIMO}}(t) = \sqrt{K/M} \sum_{p=1}^{P} \sigma_p(\theta_p)[\mathbf{c}(\theta_p) \circ \mathbf{d}(\theta_p)]^T \boldsymbol{\psi}(t) \quad (34)$$

Next, both sides of (34) are multiplied from the right by the transpose conjugate of $[\mathbf{c}(\theta_p) \circ \mathbf{d}(\theta_p)]^T \psi(t)$,

$$\sum_{p=1}^{P} \sigma_p(\theta_p) = \sqrt{M/K}[\mathbf{g}(\theta_p) \circ \mathbf{h}(\theta_p)]^H \mathbf{y}_{\text{FPMIMO}}(t) \boldsymbol{\psi}^H(t) \cdot [\mathbf{c}(\theta_p) \circ \mathbf{d}(\theta_p)]^* \quad (35)$$

Taking the average over all Q snapshots in (35), it can be obtained

$$E\left\{\sum_{p=1}^{P} \sigma_p(\theta_p)\right\} = \sqrt{M/K}[\mathbf{g}(\theta_p) \circ \mathbf{h}(\theta_p)]^H \hat{\mathbf{R}}_{\mathbf{y}\boldsymbol{\psi}} [\mathbf{c}(\theta_p) \circ \mathbf{d}(\theta_p)]^* \quad (36)$$

where $E\{\cdot\}$ denotes the averaging operator and $\hat{\mathbf{R}}_{\mathbf{y}\boldsymbol{\psi}} = E\{\mathbf{y}_{\text{FPMIMO}}(t)\psi^H(t)\} = (1/Q)\sum_{q=1}^{Q} \mathbf{y}_{\text{FPMIMO}}(q)\psi^H(q)$, so that parameter $\sigma(\theta)$ can be estimated by the LS method as:

$$\hat{\sigma}_{\text{FPMIMO}}(\theta) = \frac{\sqrt{K/M}\sum_{q=1}^{Q}(\mathbf{g}(\theta) \circ \mathbf{h}(\theta))^H \hat{\mathbf{R}}_{\mathbf{y}\boldsymbol{\psi}}(\mathbf{c}(\theta) \circ \mathbf{d}(\theta))*}{\|\mathbf{g}(\theta) \circ \mathbf{h}(\theta)\|^2 (\mathbf{c}(\theta) \circ \mathbf{d}(\theta))^T \hat{\mathbf{R}}_{\boldsymbol{\psi}\boldsymbol{\psi}}(\mathbf{c}(\theta) \circ \mathbf{d}(\theta))*} \quad (37)$$

with $\hat{\mathbf{R}}_{\boldsymbol{\psi}\boldsymbol{\psi}} = E\{\boldsymbol{\psi}(t)\boldsymbol{\psi}^H(t)\} = (1/Q)\sum_{q=1}^{Q} \boldsymbol{\psi}(q)\boldsymbol{\psi}^H(q)$.

Simplification of the denominator from (37) using (5), (6), (10), and (11) can be achieved as follows

$$\begin{aligned}\|\mathbf{g}(\theta) \circ \mathbf{h}(\theta)\|^2 &= (\mathbf{g}(\theta) \circ \mathbf{h}(\theta))^H (\mathbf{g}(\theta) \circ \mathbf{h}(\theta)) \\ &= N \|\mathbf{g}(\theta)\|^2\end{aligned} \quad (38)$$

where the last step results from $||\mathbf{h}(\theta)||^2 = N$ [22].

For the condition where $\hat{\mathbf{R}}_{\boldsymbol{\psi}\boldsymbol{\psi}} = \mathbf{I}_{M\times M}$, it can be obtained

$$(\mathbf{c}(\theta) \circ \mathbf{d}(\theta))^T \hat{\mathbf{R}}_{\boldsymbol{\psi}\boldsymbol{\psi}} (\mathbf{c}(\theta) \circ \mathbf{d}(\theta))^* = M \|\mathbf{c}(\theta)\|^2 \quad (39)$$

so that (37) simplifies into

$$\hat{\sigma}_{\text{FPMIMO}}(\theta) = \frac{\sqrt{K/M}\sum_{q=1}^{Q}(\mathbf{g}(\theta) \circ \mathbf{h}(\theta))^H \hat{\mathbf{R}}_{\mathbf{y}\boldsymbol{\psi}}(\mathbf{c}(\theta) \circ \mathbf{d}(\theta))^*}{MN \|\mathbf{g}(\theta)\|^2 \|\mathbf{c}(\theta)\|^2} \quad (40)$$

By evaluating (40), the maximum number of detectable targets for the FPMIMO radar can be obtained.

In the following we obtain $\mathbf{y}(t)$ for various waveform configurations using (9) with the number of subarrays on the Tx array being $1 < M < K$ on the Rx array $1 < N < L$. Among these configurations, only the combination of NC transmit and NC receive has been studied before, while the others are the contribution of this paper.

1) NC TRANSMIT-NC RECEIVE

For the MIMO radar, the configuration consists of a NC Tx array ($M = K$) and a NC Rx array ($N = L$). Therefore $\mathbf{a}(\theta) = \mathbf{1}_{K\times 1}$, $\mathbf{d}(\theta) = \mathbf{a}(\theta)$, $\mathbf{b}(\theta) = \mathbf{1}_{L\times 1}$, and $\mathbf{h}(\theta) = \mathbf{b}(\theta)$ so that the following is obtained,

$$\mathbf{y}(t) = \sum_{p=1}^{P} \sigma_p(\theta_p)\mathbf{b}(\theta_p)\mathbf{a}^T(\theta_p)\boldsymbol{\psi}(t) + \mathbf{n}(t) \quad (41)$$

It is observed that $\mathbf{y}(t)$ in (41) is similar to that in [13], [17].

2) NCS TRANSMIT-NC RECEIVE

For the PMIMO radar, the configuration includes a NCS Tx array ($1 < M < K$) and a NC Rx array ($N = L$). Consequently, $\mathbf{d}(\theta) = [\mathbf{a}_1(\theta), \ldots, \mathbf{a}_M(\theta)]^T$, $\mathbf{b}(\theta) = \mathbf{1}_{L\times 1}$, and $\mathbf{h}(\theta) = \mathbf{b}(\theta)$ so that it can be obtained:

$$\mathbf{y}(t) = \sqrt{K/M}\sum_{p=1}^{P} \sigma_p(\theta_p)\mathbf{b}(\theta_p)[\mathbf{c}(\theta_p) \circ \mathbf{d}(\theta_p)]^T \boldsymbol{\psi}(t) + \mathbf{n}(t) \quad (42)$$

This result is similar to that in [22], the only difference being the way in which it is written.

3) AC TRANSMIT-NC RECEIVE

The PA radar configuration consists of AC Tx array ($M = 1$) and NC Rx array ($N = L$), so that $\psi(t) = \varphi_1(t)$, $\mathbf{a}(\theta_l) = \mathbf{a}(\theta)$, $\mathbf{d}(\theta) = 1$, $\mathbf{b}(\theta) = \mathbf{1}_{L\times 1}$, and $\mathbf{h}(\theta) = \mathbf{b}(\theta)$. Hence,

$$\mathbf{y}(t) = \sqrt{K}\sum_{p=1}^{P}\sigma_p(\theta_p)\beta\mathbf{b}(\theta_p)\psi(t) + \mathbf{n}(t) \tag{43}$$

with $\beta = \mathbf{a}^T(\theta_p)\mathbf{a}(\theta_p)$.

The following is the formulation of $\hat{\sigma}(\theta)$ using (37) for various orthogonal waveform configurations with multiple subarrays on the Tx array, $1 < M < K$, and the Rx array, $1 < N < L$. The derivation of $\hat{\sigma}(\theta)$ for the PMIMO and PA radars has never been reported before.

1) NC TRANSMIT-NC RECEIVE

For the MIMO radar configuration with a NC Tx array ($M = K$) and a NC Rx array ($N = L$), we have $\mathbf{a}(\theta) = \mathbf{1}_{K\times 1}$, $\mathbf{d}(\theta) = \mathbf{a}(\theta)$, $\mathbf{b}(\theta) = \mathbf{1}_{L\times 1}$, and $\mathbf{h}(\theta) = \mathbf{b}(\theta)$ so that it is obtained

$$\hat{\sigma}(\theta) = \frac{\sum_{q=1}^{Q}\mathbf{b}^H(\theta)\hat{\mathbf{R}}_{\mathbf{y}\boldsymbol{\psi}}\mathbf{a}^*(\theta)}{\|\mathbf{b}(\theta)\|^2\,\mathbf{a}^T(\theta)\hat{\mathbf{R}}_{\boldsymbol{\psi}\boldsymbol{\psi}}\mathbf{a}^*(\theta)} \tag{44}$$

It can be seen that $\hat{\sigma}(\theta)$ in (44) is similar to that obtained in [13].

2) NCS TRANSMIT-NC RECEIVE

The PMIMO radar employs a NCS Tx array ($1 < M < K$) and a NC Rx array ($N = L$), with $\mathbf{d}(\theta) = [\mathbf{a}_1(\theta), \ldots, \mathbf{a}_M(\theta)]^T$, $\mathbf{b}(\theta) = \mathbf{1}_{L\times 1}$, and $\mathbf{h}(\theta) = \mathbf{b}(\theta)$. Therefore,

$$\hat{\sigma}(\theta) = \frac{\sqrt{K/M}\sum_{q=1}^{Q}\mathbf{b}^H(\theta)\hat{\mathbf{R}}_{\mathbf{y}\boldsymbol{\psi}}(\mathbf{c}(\theta)\circ\mathbf{d}(\theta))*}{\|\mathbf{b}(\theta)\|^2\,(\mathbf{c}(\theta)\circ\mathbf{d}(\theta))^T\hat{\mathbf{R}}_{\boldsymbol{\psi}\boldsymbol{\psi}}(\mathbf{c}(\theta)\circ\mathbf{d}(\theta))*} \tag{45}$$

3) AC TRANSMIT-NC RECEIVE

The PA radar uses an AC Tx array ($M = 1$) and a NC Rx array ($N = L$), with $\psi(t) = \varphi_1(t)$, $\mathbf{a}(\theta_l) = \mathbf{a}(\theta)$, $\mathbf{d}(\theta) = 1$, $\mathbf{b}(\theta) = \mathbf{1}_{L\times 1}$, and $\mathbf{h}(\theta) = \mathbf{b}(\theta)$. Hence,

$$\hat{\sigma}(\theta) = \frac{\sqrt{K}\sum_{q=1}^{Q}\mathbf{b}^H(\theta)\hat{\mathbf{R}}_{\mathbf{y}\psi}c*(\theta)}{\|\mathbf{b}(\theta)\|^2\,c(\theta)c*(\theta)} \tag{46}$$

From evaluation results for the maximum number of detected targets with different waveform configurations (for number of Tx subarrays $1 < M < K$ and the Rx subarrays $1 < N < L$), it is found that the maximum number of detected targets in the MIMO radar is K times greater than that in the PA radar with K antennas in the Tx array. This is shown next in Fig. 6 and Fig. 8 and also in the detailed discussion in part E of Section III, which is consistent with the results in [13].

E. PERFORMANCE EVALUATION

In evaluation of the maximum number of detectable targets for the FPMIMO radar using (37), it is assumed that the number of antennas in the T-R array is identical, $K = L = 16$ elements, while the number of subarrays varies, i.e., $1 < M < K$ in the Tx array and $1 < N < L$ in the Rx array. The spacing between antenna elements in the T-R array is half the carrier wavelength ($d_K = d_L = 0.5\lambda$). Noise is Gaussian with spatial mean of zero and the same variance in each antenna element, or $\mathbf{n}(t) \sim \mathcal{CN}(0, \sigma_n^2\mathbf{I}_{MN})$.

For evaluation of the maximum number of detectable targets of the MIMO, the PMIMO, and the PA radar, (44)–(46) are used, respectively. For the PA radar, the number of transmit subarrays is one with 16 elements. In the MIMO radar, 16 antennas produce 16 waveforms that are orthogonal to each other. In the FPMIMO radar, the number of transmit and receive subarrays might be different, the optimum values of which give relatively high T-R gain performance, as partially indicated in [28] for the PMIMO radar, and proportionally increasing number of detectable targets. The T-R gain is determined by the directional coherent gain and waveform diversity gain. The coherent gain affects the magnitude of complex amplitude, which is also an equivalent measure of the maximum target range [31], while the waveform diversity gain affects the number of detectable targets [22].

1) IMPACT OF THE NUMBER OF SUBARRAYS

The MCA for the PA radar is relatively high because it has very high directional coherent gain, which also implies a high maximum target range, relative to the other types of radar. Another consequence of the high directional coherent gain is that the minimum reflection coefficient of detectable targets is the lowest compared to the other types of radar. This is the opposite of the MIMO radar that has a high waveform diversity gain, which results in the largest maximum number of detectable targets. Meanwhile, the FPMIMO radar as the generic form of subarrayed MIMO radar can be designed to balance between the maximum number of detectable targets and the minimum reflection coefficient magnitude of detectable targets by adjusting the number of Tx-Rx subarrays (M and N). Thus, the FPMIMO radar is able to compromise between the advantage of directional coherent gain to detect small or distant targets and that of waveform diversity gain to obtain a greater number of detectable targets.

Fig. 2 depicts the performance in MCA that varies with the number of transmit subarrays M on the FPMIMO radar with $N = 16$. MCA decreases with the increasing number of transmit subarrays M. MCA for the PA radar ($M = 1$), the PMIMO radar ($M = 8$), and the MIMO radar ($M = K$), i.e. the MIMO, are 0.91, 0.79, and 0.73, respectively.

The trend of decreasing MCA with the increasing number of Tx-Rx subarrays, i.e., M and N, occurs on the FPMIMO radar in general, as shown in Fig. 3. Assuming an FPMIMO radar with conditions $M = 8$ and $M = 13$, the MCA will tend to decrease if the number of receive subarrays (N) increases. This shows that the greater value of M means that there will be as many orthogonal waveforms, which greatly determines the waveform diversity gain. This gain is also proportional to the number of detectable targets. Vice versa, if M is small, it will cause higher directional gain, which also translates to fewer detectable targets. MCA in both conditions, $M = 8$

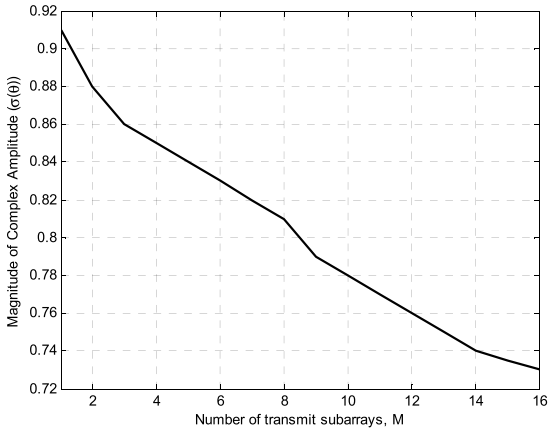

FIGURE 2. Magnitude of complex amplitude vs. number of transmit subarrays on the FPMIMO radar ($K = L = 16$, $N = 16$).

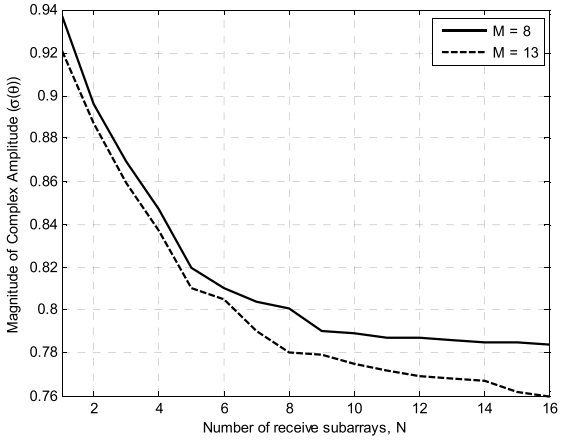

FIGURE 3. Magnitude of complex amplitude vs. number of receive subarrays on the FPMIMO radars with $K = L = 16$ for $M = 8$ and $M = 13$.

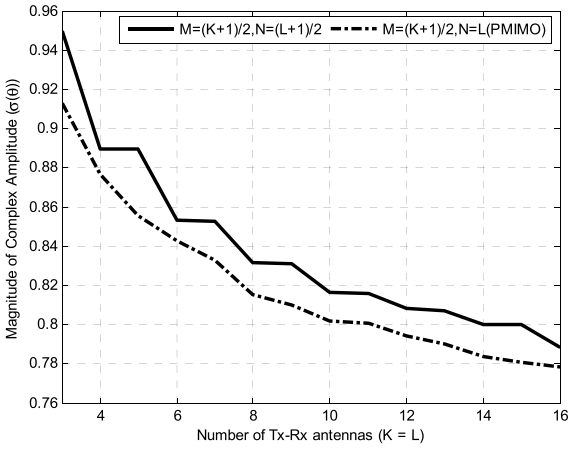

FIGURE 4. Magnitude of complex amplitude vs. number of Tx-Rx antennas.

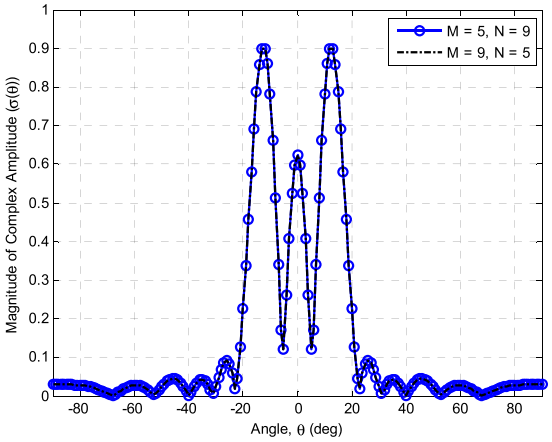

FIGURE 5. Magnitude of complex amplitude at $\theta = \{-10^o, 0^o, 10^o\}$ with $M = 5$, $N = 9$ and $M = 9$, $N = 5$ on the FPMIMO radar.

and $M = 13$, equally decreases with the increasing number of receive subarrays N, where the decrease is greater at $M = 13$. This also indicates that the use of 13 transmit subarrays provides a maximum number of detectable targets greater than that with 8 subarrays. Also seen from Fig. 3 that if greater maximum number of detectable targets is desired, then M and N must be close to the total number of antenna elements on the T-R array, i.e., K and L.

2) IMPACT OF THE TOTAL NUMBER OF ANTENNAS

In Fig. 4, two configurations with the same odd number of antennas at the Tx and Rx, $K = L$, are considered, namely a PMIMO radar with M transmit subarrays where $M = (K+1)/2$ and another case of the FPMIMO radar where $M = (K+1)/2$ and $N = (L+1)/2$. The number of Tx-Rx antennas are at least $K = L = 3$ so that overlapping subarrays can be formed. This condition is considered because it will be difficult to detect multiple targets if the number of Tx-Rx antennas are less 3. The curves of the MCA with respect to the number of T-R antennas ($K = L$) exhibit a similar decreasing trend. The MCA on the FPMIMO configuration with subarrays as many as half of the antennas is greater than on the PMIMO radar because in the latter the subarrays literally have only one element each. However, this also means that there are L waveforms formed in the receive array of the PMIMO radar, more than $(L+1)/2$ waveforms in the former. The more waveforms are formed, the higher the waveform diversity gain and the maximum number of detectable targets.

Fig. 5 shows that an identical number of detectable targets can be achieved by FPMIMO radars with reversed combinations of transmit and receive subarrays, e.g., $M = 5$, $N = 9$ with $M = 9$, $N = 5$. This also agrees with results in [21] that the two configurations exhibit equal performance in T-R gain and SINR. This property allows flexibility in the design of the FPMIMO radar, especially in achieving a good compromise between ease of design and its performance.

3) THE MAXIMUM NUMBER OF RESOLVABLE TARGETS

Table 1 presents the relation between the maximum number of detectable targets determined by the formulation of

TABLE 1. Number of detectable targets for the FPMIMO radar with $M = N = 4$ and $K = L = 8$.

P	Probability of successful detection of all targets (%)
1	100
2	100
3	100
4	90
5	70
6	50
7	20
8	10
9	0
10	0

P_{max} and the estimation of detectable target $\hat{\sigma}(\theta)$. Formulations of P_{max} for the FPMIMO and the PMIMO are given in (32)–(33) and for MIMO and the PA are given in [13, Eq. (22) and (25)], whereas the estimation of detectable target $\hat{\sigma}(\theta)$ for the FPMIMO radars is given in (37) and other radars in (44)–(46). The maximum number of detectable targets in (32) is supported by the simulation results of the estimation of detectable target $\hat{\sigma}(\theta)$ in (37). For a given number of targets P, multiple tests are carried out with different target angles. The number of detectable targets (P_{det}) is subsequently compared with P to obtain the probability of successful detection of all targets. The probabilities given in percentage in Table 1 are obtained from the mean of all tests for each value of P.

Applying (32) results in $P_{max,\text{FPMIMO}} = [3, 8]$. For $P = 1$, i.e., a single target, we experiment with ten different target directions. The test results show that all targets are detected correctly, i.e., 100% detection. Also, as shown in Table 1, for $P = 2$, i.e., two targets at two different angles, we also try ten combinations, and the test results show that all targets are still detected correctly, again 100% detection. In the same way we obtain the percentage of detectable target for $P = 3$ up to $P = 10$. The results indicate that for $1 \leq P \leq 2$ all targets can be detected properly (100% success), whereas for $3 \leq P \leq 8$ only at some of the times all targets are detected, which means the percentage of detectable target is less than 100%, while for $P > 8$ there are always some undetectable targets. These results suggest that the maximum number of detectable targets falls within the interval given in (32), which depends on the number of subarrays on transmit and receive array, i.e., M and N.

For simple validation in determining the maximum number of detectable targets on all types of FPMIMO radars, a comparison is made between the simulation results adopting the LS method for $\hat{\sigma}(\theta)$ using (37) and (44)–(46) and the calculations for P_{max} using (32)–(33) for the FPMIMO and the PMIMO and using (22) and (25) in [13] for the MIMO and the PA radars. Herein, the number of Tx-Rx antennas is set $K = L = 8$.

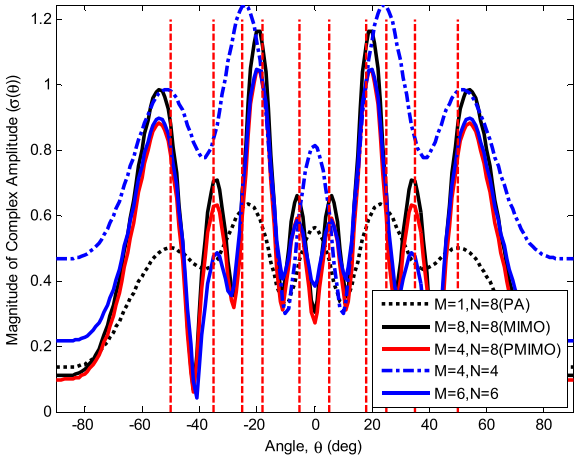

FIGURE 6. Magnitude of complex amplitude for the FPMIMO radar with variants (M, N), and $K = L = 8$, with targets at directions in Θ_A.

a: PHASED ARRAY RADAR

To determine the maximum number of detectable targets of the PA radar, it is assumed that there are 10 targets located at $\Theta_A = \{-50^o, -35^o, -25^o, -18^o, -5^o, 5^o, 18^o, 25^o, 35^o, 50^o\}$, with identical complex amplitude $\sigma_1 = \ldots = \sigma_P = 1$. We take $Q = 256$ snapshots. Signal waveforms $\psi(t)$ are the Hadamard codes designed in accordance with the number of the Tx-Rx subarrays [18]. As seen in Fig. 6 the maximum number of detectable targets for the PA radar i.e., the FPMIMO ($M = 1, N = 8$) is 4. This result is in agreement with that of P_{max} using (25) in [13] for $L = 8$, for which the number of $P_{max,\text{PA}}$ is 4. The results also indicate that six or more targets will not be completely detected by the PA radar.

b: MIMO RADAR

as an example of determination of the maximum number of detectable targets of the MIMO radar i.e., the FPMIMO with $M = 8$ and $N = 8$, it is assumed that there are 10 targets with locations and complex amplitudes as used in the preceding case. As also shown in Fig. 6, the maximum number of detectable targets of the MIMO radar is 8. This result is also in agreement with those from (22) in [13] for $K = L = 8$, for which the number of $P_{max,\text{MIMO}}$ is in [7, 32]. The results also show that the maximum number of detectable targets P_{max} of the MIMO radar is twice that of the PA radar.

c: PHASED MIMO RADAR

As an example of determination of the maximum number of detectable targets of the PMIMO radar, the same 10 targets are assumed. Result shown in Fig. 6 indicates that the maximum number of detectable targets on the particular PMIMO radar with $M = 4, N = 8$, is 8. This is in agreement with the result from (33) for $M = 4$, for which the number of $P_{max,\text{PMIMO}}$ is in the range of [5, 16].

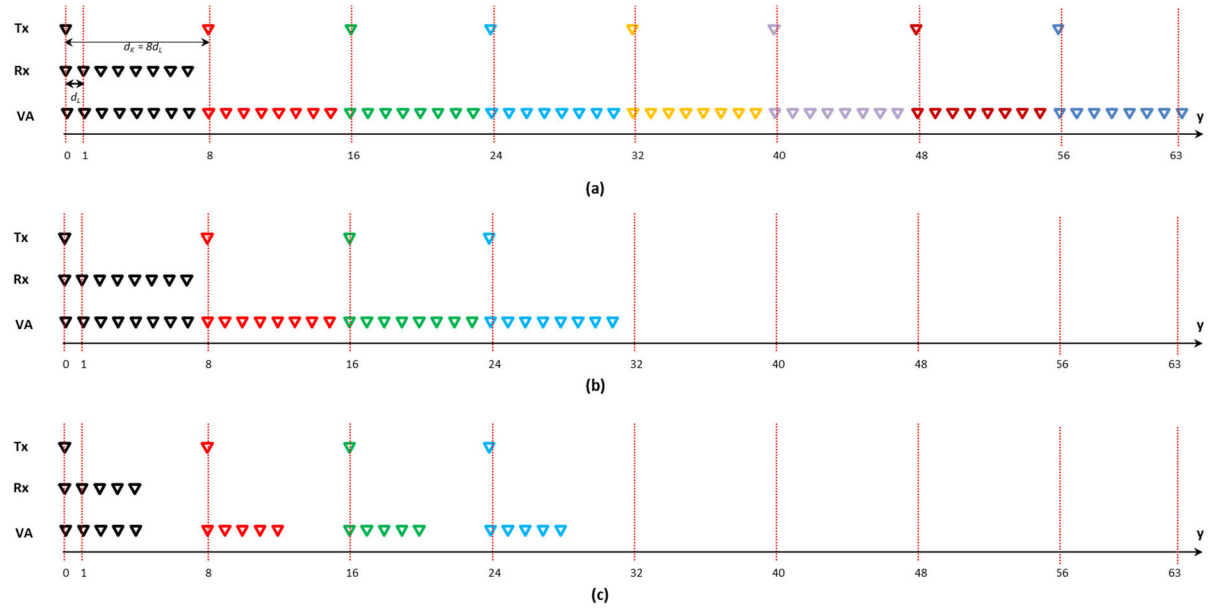

FIGURE 7. Illustration of FPMIMO antenna array with $K = L = 8$ for: (a) $M = N = 8$ (MIMO), (b) $M = 4$, $N = 8$ (PMIMO), and (c) $M = 4$, $N = 5$.

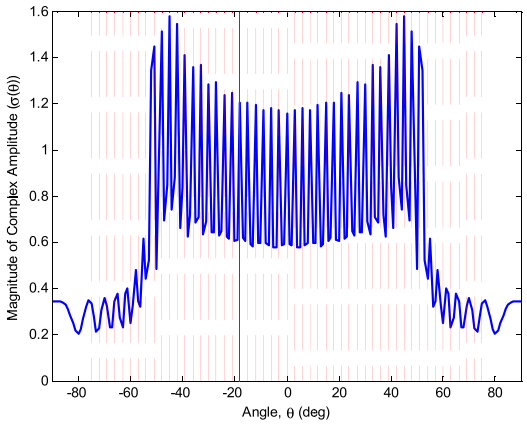

FIGURE 8. Magnitude of complex amplitude for the MIMO radar with $K = L = 8$, and $d_K = 8d_L$, with targets at angles in Θ_B.

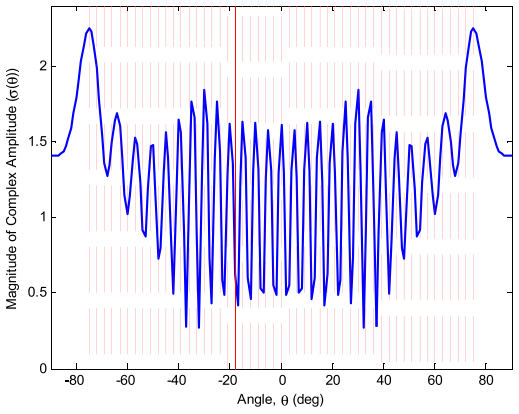

FIGURE 9. Magnitude of complex amplitude for the PMIMO radar with $M = 4$, $K = L = 8$, and $d_K = 8d_L$, with targets at angles in Θ_B.

d: OTHER FPMIMO CONFIGURATIONS

The same exercise can be done for other configurations of FPMIMO radar for the same 10 targets. As also seen in Fig. 6 the maximum number of detectable targets on the FPMIMO structure with ($M = 4$, $N = 4$) and ($M = 6$, $N = 6$) are 5 and 8, respectively, which is in agreement with the results from (32) for these two variants, for which the numbers of $P_{max,\text{FPMIMO}}$ are [3, 8] and [5, 18], respectively.

4) IMPACT OF ELEMENT SPACING

With $K = L = 8$, the largest P_{max} is $8 \times 8 = 64$ so that the spacing between elements in the Tx array is $d_K = 8d_L = 4\lambda$ [13], [17]. The number of VA elements corresponds with the configurations of the Tx and Rx arrays [17], as presented in Fig. 7 for several combinations of (M, N) for $K = L = 8$. To evaluate the maximum number of detectable targets of the MIMO radar with $d_K = 8d_L$ and $d_L = 0.5\lambda$ it is assumed that there are 51 targets located at $\Theta_B = \{-75^o, -72^o, -69^o, \ldots, -3^o, 0^o, 3^o, \ldots, 69^o, 72^o, 75^o\}$, with identical complex amplitude $\sigma_1 = \ldots = \sigma_P = 1$. Fig. 8 indicates that the maximum number of detectable targets of the MIMO radar with $K = L = 8$ is 47. The result also shows that the P_{max} obtained for the MIMO radar is more than eleven times that for the PA radar. This result agrees with that reported in [13].

For the PMIMO radar we assume the same antenna spacings as in the previous MIMO case with the same P targets. Fig. 9 demonstrates that the maximum number of detectable targets for the PMIMO radar with ($M = 4$, $N = 8$) is 25, which indicates that the maximum number of detectable

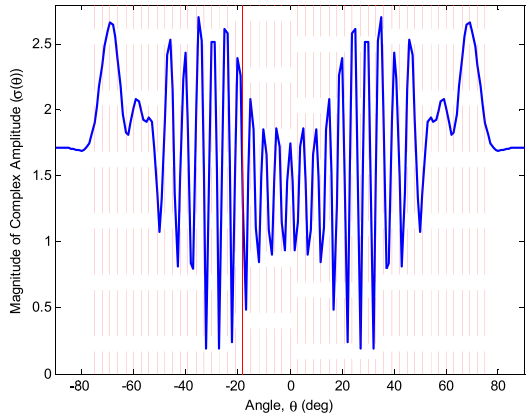

FIGURE 10. Magnitude of complex amplitude for the FPMIMO radar with $M = 4$, $N = 5$, $K = L = 8$, and $d_K = 8d_L$, with targets at angles in Θ_B.

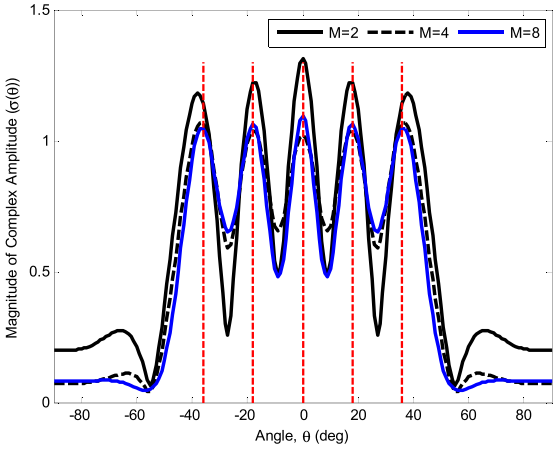

FIGURE 11. Magnitude of complex amplitude for the FPMIMO radar ($N = 8$, $K = L = 8$) with varying the number of transmit subarrays (M) with targets at angles in Θ_C.

targets for the PMIMO radar is more than six times that for the PA radar. Likewise, for a configuration with the same antenna spacings and targets where $M = 4$ and $N = 5$, Fig. 10 shows that the maximum number of detectable targets is 19, which is more than four times the value for the PA configuration.

5) ACCURACY OF DETECTION

The detection accuracy of the FPMIMO radar turns out to be determined by the number of subarrays in the Tx-Rx array as presented in Fig. 11 and Fig. 12. In this example, the FPMIMO radar has inter-element spacings in the T-R array $d_K = d_L = 0.5\lambda$ with $K = L = 8$. It is assumed that $\Theta_C = \{-36^o, -18^o, 0^o, 18^o, 36^o\}$ with identical complex amplitude $\sigma_1 = \ldots = = \sigma_5 = 1$. In Fig. 11, for the FPMIMO radar with $N = 8$, when the number of transmit subarrays (M) increases, the accuracy of detectable target is increasing. Detection errors of 2^o and 1^o for M equal to 2 and 4, respectively, only occur at $\theta = \pm 36^o$, whereas for $M = 8$, the targets are detected correctly. This indicates

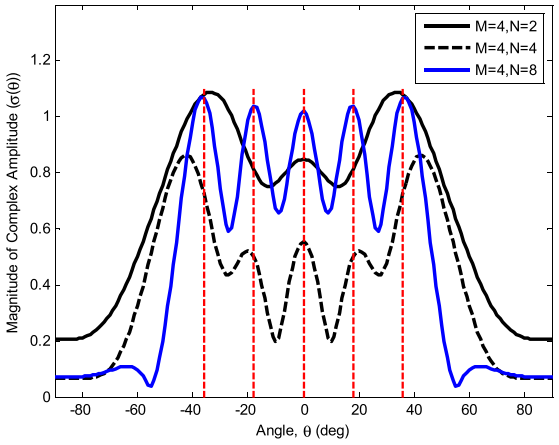

FIGURE 12. Magnitude of complex amplitude for the FPMIMO ($M = 4$, $K = L = 8$) radar with varying number of receive subarrays (N) with targets at angles in Θ_C.

that increasing the number of transmit subarrays will increase the accuracy of target detection. All targets can be detected by increasing the number of receive subarrays (N) as shown in Fig. 12. It also appears that for the FPMIMO radar with $M = 4$, all targets can only be detected at $N = 8$ although there is still an error in detection. Thus, the number of Tx-Rx subarrays (M and N) greatly determines the number and accuracy of detectable targets because it affects the size of the T-R aperture on the Tx-Rx array of antennas, in agreement with [19].

The accuracy of angle detection is largely determined by the radar VA mentioned in [17]. In Fig. 11, if $\mathcal{N}_{\text{FPMIMO}}$ is obtained with (16) then the FPMIMO radars with $N = 8$ and $M = \{2, 4, 8\}$ has$\mathcal{N} = \{9, 11, 15\}$. This shows that the configuration of FPMIMO radar with ($M = N = 8$), i.e., the MIMO radar, has the accuracy of target detection that outperforms other configurations since it has the largest N. Through similar analysis for Fig. 12, the FPMIMO radars with $M = 4$ and $N = \{2, 4, 8\}$ result in$\mathcal{N} = \{5, 7, 11\}$ which implies that the highest accuracy of detection belongs to the configuration with the largest N, namely the ($M = 4, N = 8$) structure, known as the PMIMO radar.

In Fig. 12, several cases of the FPMIMO radar are compared, one of which is the PMIMO radar structure with $M = 4, N = 8$. The use of overlapping subarrays on the FPMIMO radar results in highly directional coherent gain that is proportional to the high MCA, but also reduces the number of detectable targets. The high MCA is very helpful for detecting targets with small RCS or weak reflection. However, this is in contrast to the MIMO radar condition where each element on the Tx array has a waveform, which is essentially equivalent to non-overlapping transmit subarrays with one element in each subarray.

The above cases demonstrate the flexibility of the FPMIMO structure in trading off between coherent gain and waveform diversity gain, which in turn determines the maximum number of detectable targets.

IV. DETECTION AND FALSE ALARM PROBABILITIES

A. REVIEW OF TARGET DETECTION OF THE PA AND MIMO RADAR

The following review, summarized mostly from [32], is provided to give better clarity to discussions in the sequel on the detection performance. Performance indicators of target detection as reported in [32] are the probability of detection (P_d), the probability of miss detection (P_m), and the probability of false alarm (P_{fa}). For the MIMO radar, these parameters are [32]

$$P_{fa,\mathrm{MIMO}} = \exp\left(\frac{-\eta_{\mathrm{MIMO}}}{KL\sigma_n^2}\right) \tag{47}$$

$$P_{d,\mathrm{MIMO}} = \exp\left(\frac{\ln(P_{fa,\mathrm{MIMO}})}{1+KL(SNR)}\right) \tag{48}$$

$$P_{m,\mathrm{MIMO}} = 1 - P_{d,\mathrm{MIMO}} \tag{49}$$

$$SNR = \frac{\sigma_p^2}{\sigma_n^2} \tag{50}$$

$$\eta_{\mathrm{MIMO}} = \frac{(KL\sigma_p^2+\sigma_n^2)\sigma_n^2}{\sigma_p^2}\ln\left(\frac{(KL\sigma_p^2+\sigma_n^2)V_T}{\sigma_n^2}\right) \tag{51}$$

where σ_p^2 and σ_n^2 denote the target signal and the noise power, respectively, and V_T denotes the threshold value that is used to determine the target detection and set according to the desired false alarm rate [7], [18], [32].

On the other hand, the parameters of the target detection for the PA radar are [32]

$$P_{fa,\mathrm{PA}} = \exp\left(\frac{-\eta_{\mathrm{PA}}}{KL\sigma_n^2}\right) \tag{52}$$

$$P_{d,\mathrm{PA}} = \exp\left(\frac{\ln(P_{fa,\mathrm{PA}})}{1+K^2L(SNR)}\right) \tag{53}$$

$$P_{m,\mathrm{PA}} = 1 - P_{d,\mathrm{PA}} \tag{54}$$

$$\eta_{\mathrm{PA}} = \frac{(K^2L\sigma_p^2+\sigma_n^2)\sigma_n^2}{K\sigma_p^2}\ln\left(\frac{(K^2L\sigma_p^2+\sigma_n^2)V_T}{\sigma_n^2}\right) \tag{55}$$

B. TARGET DETECTION OF THE FPMIMO RADAR

As in the derivation of target detection performance criteria for the PA and MIMO radars in [32], the detection problems on the FPMIMO radar are formulated as follows

$$\begin{aligned} H_0 &: \mathbf{u} = \mathbf{n} \\ H_1 &: \mathbf{u} = \sqrt{\frac{K}{M}}\sigma_p\mathbf{e}(\theta) + \mathbf{n} \end{aligned} \tag{56}$$

where $\mathbf{u}$ and $\mathbf{e}(\theta)$ are defined in (12) and (13), respectively, H_0 and H_1 are the hypotheses that there is only noise (no echo signal) in $\mathbf{u}$ and that $\mathbf{u}$ contains an echo signal, respectively. For the target echoes and the noise, it is assumed $\sigma_p \sim \mathcal{CN}(0, \mathbf{I_{MN}})$ and $\mathbf{n} \sim \mathcal{CN}(0, \sigma_{\mathbf{n}}^2\mathbf{I}_{MN})$.

The optimum solution for hipothesis testing with Neyman-Pearson, namely, the likelihood ratio test (LRT), requires the knowledge of the probability distribution of $\mathbf{e}(\theta)$. In (56) the distribution of σ_p is known but it is not the case for θ and, hence, the distribution of $\mathbf{e}(\theta)$ is unknown. Therefore, the detection problem becomes maximum likelihood (ML) estimation given as

$$\frac{\max\limits_{e(\theta)} P(u\,|H_1, \sigma_n^2, e(\theta))}{P(u\,|H_0, \sigma_n^2)} \underset{<_{H_0}}{\overset{>}{}}^{H_1} V_T \tag{57}$$

The probability density for $\mathbf{u}$ with respect to H_1 can be expressed as

$$\begin{aligned} &P(\mathbf{u}\,|H_1, \sigma_n^2, \mathbf{e}(\theta)) \\ &= \pi^{-MN}\sigma_n^{-2MN} \\ &\quad\times \exp\left(-\left(\mathbf{u}-\sqrt{\frac{K}{M}}\sigma_p\mathbf{e}(\theta)\right)^H\left(\mathbf{u}-\sqrt{\frac{K}{M}}\sigma_p\mathbf{e}(\theta)\right)\sigma_n^{-2}\right) \end{aligned} \tag{58}$$

By taking the natural logarithm of (58), differentiating the result with respect to $\mathbf{e}(\theta)$ and equating it to zero, we obtain the ML estimate as

$$\widehat{e}(\theta) = \sqrt{\frac{M}{K}}\mathbf{u} \tag{59}$$

When the estimate $\widehat{e}(\theta)$ in (59) is substituted into (58) for $\mathbf{e}(\theta)$, the distribution becomes

$$P(\mathbf{u}\,|H_1, \sigma_n^2, \mathbf{e}(\theta)) = \pi^{-MN}\sigma_n^{-2MN} \tag{60}$$

and the probability density of $\mathbf{u}$ with respect to H_0 is expressed by

$$P(\mathbf{u}\,|H_0, \sigma_n^2) = \pi^{-MN}\sigma_n^{-2MN}\exp\left(-\frac{\mathbf{u}^H\mathbf{u}}{\sigma_n^2}\right) \tag{61}$$

then the log likelihood ratio is stated by

$$\ln\left(\frac{P(\mathbf{u}\,|H_1, \sigma_n^2, \mathbf{e}(\theta))}{P(\mathbf{u}\,|H_0, \sigma_n^2)}\right) = -\frac{\mathbf{u}^H\mathbf{u}}{\sigma_n^2} \tag{62}$$

so the LRT becomes

$$\|\mathbf{u}\|^2 \underset{<_{H_0}}{\overset{>}{}}^{H_1} \eta_{\mathrm{FPMIMO}} \tag{63}$$

where

$$\eta_{\mathrm{FPMIMO}} = \sigma_n^2\ln(V_T) \tag{64}$$

Again, the optimal detector for Neyman-Pearson criteria in FPMIMO radar corresponds with the noncoherent summation of the MF output when direction θ of the signal is unknown. To evaluate the target detection performance of the FPMIMO radar, we assume that the distribution of θ is known so that $\mathbf{e}(\theta)$ in (56) can be substituted with the MF output. As such, the elements of vector $\mathbf{e}(\theta)$ become identical and, hence, coherent integration can be performed before the detection process by multiplying the received signal vector in (12) with $[(\mathbf{g}(\theta)\bigcirc\mathbf{h}(\theta))\otimes(\mathbf{c}(\theta)\bigcirc\mathbf{d}(\theta))]^H$ [31]. Afterward, the detection problem becomes

$$\begin{aligned} H_0 &: u = n \\ H_1 &: u = \sqrt{\frac{K}{M}}K_M L_N MN\sigma_p + n \end{aligned} \tag{65}$$

where $n \sim \mathcal{CN}(0, K_M L_N MN\sigma_n^2)$ so the LRT solution in (65) becomes

$$\frac{P(u\,|H_1, \sigma_n^2, \sigma_p^2)}{P(u\,|H_0, \sigma_n^2)} \underset{<_{H_0}}{\overset{>_{H_1}}{}} V_T \tag{66}$$

Since the distributions of $\mathbf{e}(\theta)$ and $\mathbf{n}$ are known, the probability density of $\mathbf{u}$ given H_1 can be expressed as

$$P(u\,|H_1, \sigma_n^2, \sigma_p^2) = \frac{1}{\pi K_M L_N MN[(K/M)K_M L_N MN\sigma_p^2 + \sigma_n^2]} \times \exp\left(-\frac{|u|^2}{K_M L_N MN[(K/M)K_M L_N MN\sigma_p^2 + \sigma_n^2]}\right) \tag{67}$$

and the probability density of $\mathbf{u}$ with respect to H_0 is expressed by

$$P(u\,|H_0, \sigma_n^2) = \frac{1}{\pi K_M L_N MN\sigma_n^2} \times \exp\left(-\frac{|u|^2}{K_M L_N MN\sigma_n^2}\right) \tag{68}$$

then the log likelihood ratio is stated by

$$|u|^2 \underset{<_{H_0}}{\overset{>_{H_1}}{}} \eta_{\text{FPMIMO}} \tag{69}$$

with

$$\eta_{\text{FPMIMO}} = \frac{(KK_M L_N MN\sigma_p^2 + M\sigma_n^2)\sigma_n^2}{K\sigma_p^2} \times \ln\left(\frac{(KK_M L_N MN\sigma_p^2 + M\sigma_n^2)V_T}{M\sigma_n^2}\right) \tag{70}$$

When the target is absent then the distribution of $|u|^2$ is exponential, i.e.,

$$|u|^2 \sim \exp\left(\frac{1}{K_M L_N MN\sigma_n^2}\right) \tag{71}$$

so that the probability of false alarm of the FPMIMO radar is

$$P_{fa,\text{FPMIMO}} = P\left(\exp\left(\frac{1}{K_M L_N MN\sigma_n^2}\right) > \eta_{\text{FPMIMO}}\right) = \exp\left(\frac{-\eta_{\text{FPMIMO}}}{K_M L_N MN\sigma_n^2}\right) \tag{72}$$

with the threshold

$$\eta_{\text{FPMIMO}} = K_M L_N MN\sigma_n^2 \ln\left(\frac{1}{P_{fa,\text{FPMIMO}}}\right) \tag{73}$$

However, if the target is present, the distribution of $|u|^2$ is exponential, i.e.,

$$|u|^2 \sim \exp\left(\frac{1}{K_M L_N MN[(K/M)K_M L_N MN\sigma_p^2 + \sigma_n^2]}\right) \tag{74}$$

so that the probability of detection is

$$P_{d,\text{FPMIMO}} = \exp\left(\frac{-\eta_{\text{FPMIMO}}}{K_M L_N MN[(K/M)K_M L_N MN\sigma_p^2 + \sigma_n^2]}\right) \tag{75}$$

By substituting η_{FPMIMO} in (73) into (75), we obtain

$$P_{d,\text{FPMIMO}} = \exp\left(\frac{M\sigma_n^2 \ln(P_{fa,\text{FPMIMO}})}{KK_M L_N MN\sigma_p^2 + M\sigma_n^2}\right) \tag{76}$$

The probability of miss detection, i.e.,

$$P_{m,\text{FPMIMO}} = 1 - P_{d,\text{FPMIMO}} \tag{77}$$

If SNR is defined in (50), then (76) will be

$$P_{d,\text{FPMIMO}} = \exp\left(\frac{M \ln(P_{fa,\text{FPMIMO}})}{M + KK_M L_N MN(SNR)}\right) \tag{78}$$

The above expressions for detection performance of the FPMIMO radar are the contribution of this paper. The following expressions are obtained for η, P_{fa}, and P_d for various configurations using (70), (72), and (78) with $1 \le M \le K$ subarrays on the transmit array and $1 \le N \le L$ subarrays on the receive array.

1) NC TRANSMIT-NC RECEIVE

The MIMO radar configuration consists of a NC Tx array ($M = K$) and a NC Rx array ($N = L$) so that the following is obtained,

$$\eta = \frac{(KL\sigma_p^2 + \sigma_n^2)\sigma_n^2}{\sigma_p^2} \ln\left(\frac{(KL\sigma_p^2 + \sigma_n^2)V_T}{\sigma_n^2}\right) \tag{79}$$

$$P_{fa} = \exp\left(\frac{-\eta}{KL\sigma_n^2}\right) \tag{80}$$

$$P_d = \exp\left(\frac{\ln(P_{fa})}{1 + KL(SNR)}\right) \tag{81}$$

Expressions in (79)–(81) are in line with the results obtained in (51), (47), and (48).

2) NCS TRANSMIT-NC RECEIVE

The PMIMO radar configuration includes a NCS Tx array ($1 < M < K$) and a NC Rx array ($N = L$) so that it can be obtained:

$$\eta = \frac{(KK_M ML\sigma_p^2 + M\sigma_n^2)\sigma_n^2}{K\sigma_p^2} \times \ln\left(\frac{(KK_M ML\sigma_p^2 + M\sigma_n^2)V_T}{M\sigma_n^2}\right) \tag{82}$$

$$P_{fa} = \exp\left(\frac{-\eta}{K_M ML\sigma_n^2}\right) \tag{83}$$

$$P_d = \exp\left(\frac{M \ln(P_{fa})}{M + KK_M ML(SNR)}\right) \tag{84}$$

3) AC TRANSMIT-NC RECEIVE

The PA radar configuration consists of an AC Tx array ($M = 1$) and a NC Rx array ($N = L$), and therefore,

$$\eta = \frac{(K^2 L\sigma_p^2 + \sigma_n^2)\sigma_n^2}{K\sigma_p^2} \ln\left(\frac{(K^2 L\sigma_p^2 + \sigma_n^2)V_T}{\sigma_n^2}\right) \quad (85)$$

$$P_{fa} = \exp\left(\frac{-\eta}{KL\sigma_n^2}\right) \quad (86)$$

$$P_d = \exp\left(\frac{\ln(P_{fa})}{1 + K^2 L(SNR)}\right) \quad (87)$$

Expressions in (85)–(87) are similar to (55), (52) and (53).

These expressions reveal that the threshold value, the probability of false alarm, and the probability detection form a one-to-one relationship. This indicates that the optimal determination of the threshold determines the success of radar system's target detection.

C. PERFORMANCE EVALUATION

In this section, we compare numerically the performance of target detection for various radar configurations. The performance of target detection on the FPMIMO radar is given by (72) and (78) for P_{fa} and P_d, respectively, assuming that the number of antennas in the Tx-Rx array is identical, $K = L = 8$ elements, while the number of subarrays varies, i.e. $1 < M < K$ in the Tx array and $1 < N < L$ in the Rx array. The special cases of MIMO, PA and PMIMO structure are evaluated using (80), (86), and (83) for P_{fa} and using (81), (87), and (84) for P_d.

1) IMPACT OF THE THRESHOLD VALUE

The threshold is set to produce tolerable values of P_{fa} since too low a value of P_{fa} might sacrifice P_m. The value of P_d is dependent on P_{fa} and complementary to P_m. Accordingly, the detection performance of radar system is usually presented in P_d and P_{fa}, also known as the receiver operation characteristic (ROC). Fig. 13 shows the effect of the increase of V_T on P_d and P_{fa}.

Suppose the target reflection coefficient $\sigma_p = 1$, and accordingly, the target signal power $\sigma_p^2 = 1$, with white Gaussian noise of power $\sigma_n^2 = 0.1$, so that SNR is 10 dB. The detection performance of the radar system is presented in P_d and P_{fa} each as a function of V_T in the range of 0-35. The antenna array is assumed to be linear with $K = L = 8$, then evaluation of the detection performance is carried out for the FPMIMO radar in five configurations, i.e., ($M = 3, N = 6$), ($M = 6, N = 3$), the PMIMO radar ($M = 4, N = 8$), the PA radar ($M = 1, N = 8$), and the MIMO radar ($M = N = 8$).

Fig. 13a shows that the PA radar outperforms the MIMO radar in terms of P_{fa}, for both of which the performance is better when V_T is greater. The PMIMO radar has the P_{fa} performance between the PA and the MIMO radar. The FPMIMO radar with ($M = 6, N = 3$) has the P_{fa} performance between the PA and the PMIMO radar but the FPMIMO with ($M = 3, N = 6$) outperforms the other radars. This shows the ability of the FPMIMO radar to adjust the

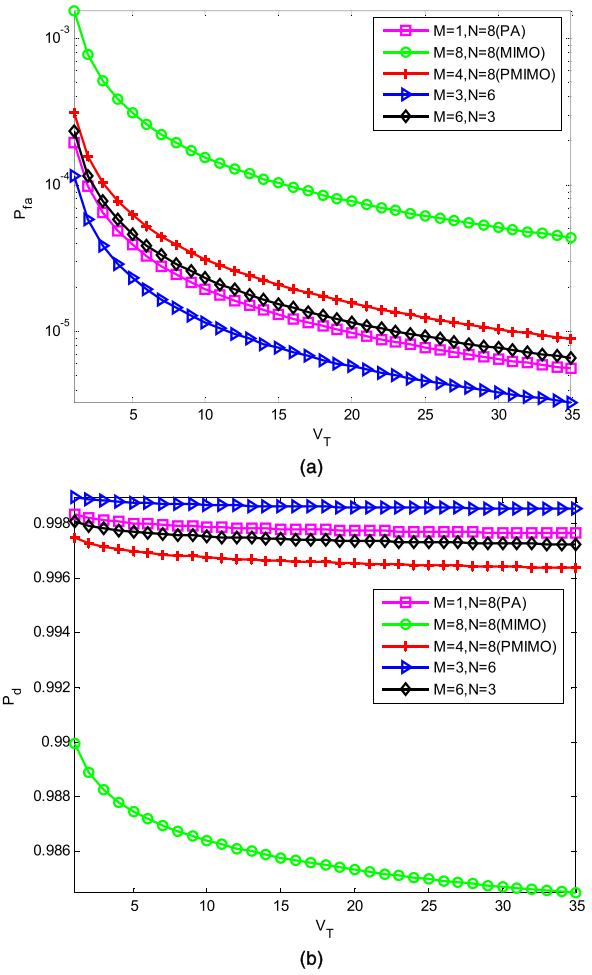

FIGURE 13. The detection performance vs. threshold (V_T) for all radar variations in: (a) the probability of false alarm (P_{fa}) and (b) the probability of detection (P_d).

performance of the P_{fa} based on the conditions of the desired target. The P_{fa} value for all radar systems is below 10^{-4} for V_T over 30.

Fig. 13b demonstrates that the ($M = 3, N = 6$) configuration outperforms the others, because P_d is a function of P_{fa}. In overall, the detection probability performance of all configurations is still within the limits of tolerance, which is greater than 97%, with the corresponding probability of false alarm smaller than 10^{-4} when the threshold is greater than 30, in agreement with results in [33] and [34]. Based on these results, in the next evaluation V_T is set to 30, since smaller V_T yields sub-optimal detection performance.

2) IMPACT OF THE SNR

In [32], the PA radar outperforms the MIMO radar in detection probability at low SNR. However, the situation is reversed at high SNR. Herein we evaluate the detection probability performance of the FPMIMO radar as a function of SNR in relation to the performance of the special cases of PA and MIMO radars given in [32]. All configuration parameters are assumed as before. The detection probability of all

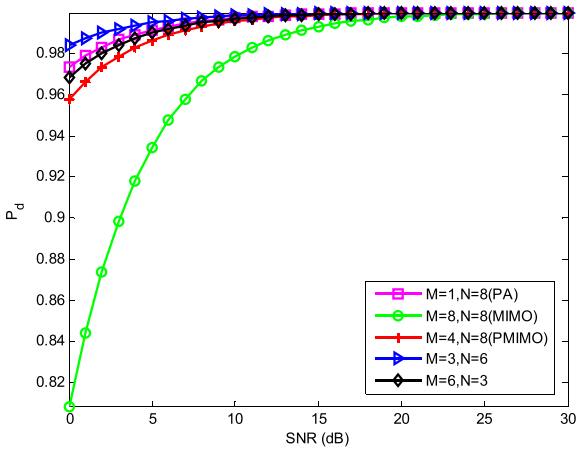

FIGURE 14. The probability of detection vs. SNR for all radar variations with $P_{fa} = 10^{-6}$.

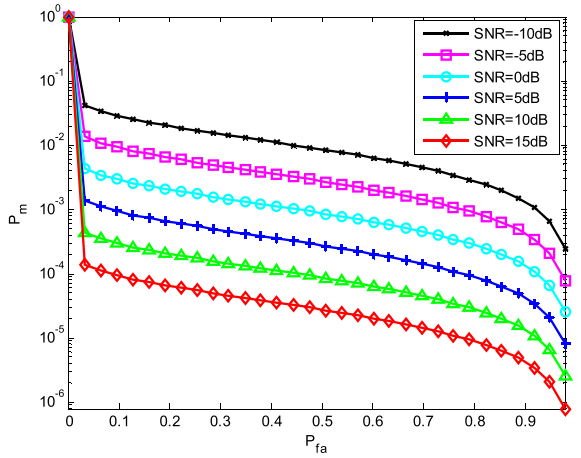

FIGURE 15. The probability of miss detection vs. P_{fa} for the FPMIMO radar ($M = N = 4$) with the variation of SNR.

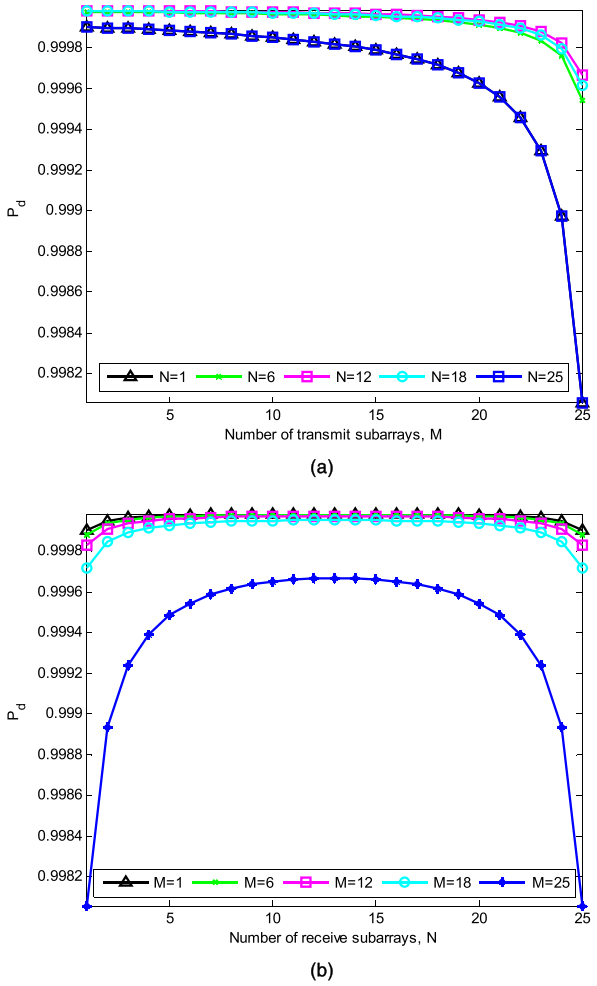

FIGURE 16. The probability of detection of the FPMIMO radar with $V_T = 30$, $\sigma_p^2 = 1$, and $\sigma_n^2 = 0.1$ as: (a) the function of number of transmit subarrays (M) and (b) as function of the number of receive subarrays (N).

configurations is evaluated for SNR in the 0-30 dB range, while P_{fa} is set to 10^{-6}. The results shown in Fig. 14 confirm those in [32] that the PA configuration outperforms the others in detection probability at low SNR. For SNR up to 10 dB, it is shown that all types of the SMIMO radar, such as those with ($M = 4, N = 8$) i.e., the PMIMO, with ($M = 3, N = 6$), and with ($M = 6, N = 3$), provide the value of P_d greater than 99%. This indicates that target detection is optimal for the SNR above 10 dB. Especially if the P_{fa} is set to greater than 10^{-6}, the performance of P_d is better for SNR less than 10 dB [37].

Fig. 15 shows the performance of P_m on the FPMIMO radar with ($M = N = 4$) and $K = L = 8$ as a function of the P_{fa}. It shows that for SNR greater than 10 dB, the FPMIMO radar exhibits the miss probability smaller than 10^{-4} that corresponds with false alarm probability less than 10^{-4}. This indicates that the false alarm rate P_{fa} that provides the optimal detection probability P_d is smaller than 10^{-4}. Since P_m is a complement of P_d, with a small P_m the performance of P_d is better.

3) IMPACT OF THE NUMBER OF SUBARRAYS

If V_T, P_{fa}, and SNR are fixed then the advantage of the FPMIMO radar, in the form of adaptability of the number of subarrays in Tx and Rx, can be exploited to achieve the desired multi-criteria performance.

In Fig. 16, the FPMIMO radar takes on $K = L = 25$ and $V_T = 30$, with SNR = 10 dB. The detection probability P_d as a function of number of transmit subarrays M with respect to $N = \{1, 6, 12, 18, 25\}$ is presented in Fig. 16a. It appears that for a given M, P_d is higher if $N \approx L/2$. For any N, the detection performance for the FPMIMO radar is decreasing with increasing M. Especially at $N = 1$ and $N = 25$, the decline in the detection performance is faster than at other N. The results also show that, the closer the number of receive subarrays to $N = L/2$, the better the detection performance. This can also be explained by the fact that the independent receive elements and the orthogonal waveforms altogether provide the VA, the size of which is proportional to the maximum number of detectable targets.

Unlike the results in Fig. 16a, Fig. 16b shows a symmetrical up and down trend in P_d with respect to N.

TABLE 2. Summary of performance of FPMIMO radar with variants (M, N) pairs.

Parameter	$M = 1, N = L$ (PA)	$M = K, N = L$ (MIMO)	$1 < M < K, N = L$ (PMIMO)	$1 < M < K, 1 < N < L$
G_{TR}	K [22]	1 [22]	$(M/K)^2 K_M^2$ [22]	$(M/K)^2 (N/L)^2 K_M^2 L_N^2$ [31]
SNR	K [22]	1 [22]	K_M [22]	$(N/L)K_M L_N$ [31]
SIR	1 [22]	1 [22]	$(M/K)K_M$ [22]	$(M/K)(N/L)K_M L_N$ [31]
R_{max}	$(K)^{1/4}$ [22]	1 [22]	$[(M/K)K_M^2]^{1/4}$ [22]	$[(M/K)(N/L)^2 K_M^2 L_N^2]^{1/4}$ [31]
$\hat{\sigma}(\theta)$	$\frac{K^{1/2}\sum_{q=1}^{Q}\mathbf{b}^H(\theta)\hat{\mathbf{r}}_{y\psi}c^*(\theta)}{\lVert\mathbf{b}(\theta)\rVert^2 c(\theta)c^*(\theta)}$	$\frac{\sum_{q=1}^{Q}\mathbf{b}^H(\theta)\hat{\mathbf{R}}_{y\psi}\mathbf{a}^*(\theta)}{\lVert\mathbf{b}(\theta)\rVert^2\mathbf{a}^T(\theta)\hat{\mathbf{R}}_{\psi\psi}\mathbf{a}^*(\theta)}$ [13]	$\frac{(K/M)^{1/2}\sum_{q=1}^{Q}\mathbf{b}^H(\theta)\hat{\mathbf{R}}_{y\psi}(\mathbf{c}(\theta)\circ\mathbf{d}(\theta))^*}{\lVert\mathbf{b}(\theta)\rVert^2(\mathbf{c}(\theta)\circ\mathbf{d}(\theta))^T\hat{\mathbf{R}}_{\psi\psi}(\mathbf{c}(\theta)\circ\mathbf{d}(\theta))^*}$ [30]	$\frac{(K/M)^{1/2}\sum_{q=1}^{Q}(\mathbf{g}(\theta)\circ\mathbf{h}(\theta))^H\hat{\mathbf{R}}_{y\psi}(\mathbf{c}(\theta)\circ\mathbf{d}(\theta))^*}{\lVert\mathbf{g}(\theta)\circ\mathbf{h}(\theta)\rVert^2(\mathbf{c}(\theta)\circ\mathbf{d}(\theta))^T\hat{\mathbf{R}}_{\psi\psi}(\mathbf{c}(\theta)\circ\mathbf{d}(\theta))^*}$
P_{max}	$\left\lceil\frac{L-1}{2}\right\rceil$ [13]	$\left[\frac{K+L-2}{2},\frac{KL+1}{2}\right)$ [13]	$\left[\frac{M+L-2}{2},\frac{ML+1}{2}\right)$	$\left[\frac{M+N-2}{2},\frac{MN+1}{2}\right)$
$\mathcal{N}$	L [13]	$[K+L-1, KL]$ [13]	$[M+L-1, ML]$	$[M+N-1, MN]$
P_{fa}	$\exp\left(\frac{-\eta}{KL\sigma_n^2}\right)$ [32]	$\exp\left(\frac{-\eta}{KL\sigma_n^2}\right)$ [32]	$\exp\left(\frac{-\eta}{K_M ML\sigma_n^2}\right)$	$\exp\left(\frac{-\eta}{K_M L_N MN\sigma_n^2}\right)$
P_d	$\exp\left(\frac{\ln(P_{fa})}{1+K^2L(SNR)}\right)$ [32]	$\exp\left(\frac{\ln(P_{fa})}{1+KL(SNR)}\right)$ [32]	$\exp\left(\frac{M\ln(P_{fa})}{M+KK_M ML(SNR)}\right)$	$\exp\left(\frac{M\ln(P_{fa})}{M+KK_M L_N MN(SNR)}\right)$

Note: G_{TR}, SNR, SIR, and R_{max} are normalized to the MIMO parameters.

For all variations of $M = \{1, 6, 12, 18, 25\}$, the performance of P_d increases dramatically until $N = L/2$, which in the case of $L = 25$ takes the value of 12 and 13. This increases P_d over 99% before the drop that is symmetrical to the earlier rise. As M increases, P_d decreases. This indicates that the FPMIMO radar with certain N and $K = L$ produces high performance in P_d for small M. This also shows that the configuration with $K = L = 8$ as reported by [31] has fulfilled the requirements in detection performance.

V. CONSIDERATIONS FOR IMPLEMENTATION AND APPLICATIONS

A. ADAPTABLE SUBARRAYED MIMO RADAR

Results of the FPMIMO radar performance evaluation with various subarray configurations, especially in terms of the maximum number of detectable targets (P_{max}), the complex amplitude of target echo ($\hat{\sigma}(\theta)$), the angular resolution, the number of elements in virtual arrays (N), the probability of false alarm (P_{fa}), the probability of detection (P_d), and so on, as well as the results reported in [31] for the T-R gain (G_{TR}), the SNR, the SIR, and the maximum range (R_{max}), indicate that the FPMIMO radar provides a generic structure of the subarrayed multi-antenna radar structure. This was achieved by the ability of the FPMIMO radar to exploit the number of overlapped subarrays on each of the Tx and Rx arrays, i.e., M and N, so that orthogonal waveforms can be transmitted by $1 \leq M \leq K$ subarrays and echo signals from targets received by $1 \leq N \leq L$ subarrays independently. With this capability, the FPMIMO radar can serve as a flexible SMIMO radar by its capability in adjusting M and N to obtain the performance parameters that cater to the desired conditions of the targets at that time.

Being a generic form, when necessary, the FPMIMO radar can enjoy the main advantage of the PA radar (i.e., coherent directional gain), the MIMO radar (i.e., waveform diversity gain), or the PMIMO radar (i.e., SINR gain). This can be obtained because the PA radar is a FPMIMO radar with ($M = 1, N = L$), while the MIMO radar is one with ($M = K$, $N = L$), and the PMIMO radar is another with ($1 \leq M \leq K$, $N = L$).

In [31] a comparison of the performance of the FPMIMO radars with different configurations has been reported for such parameters as G_{TR}, SNR, SIR, and R_{max}, as presented in Table 2. Table 2 also presents the latest comparison results of the FPMIMO radar performance for parameters such as $\hat{\sigma}(\theta)$, P_{max}, N, P_d, and P_{fa}, which are the contribution of this paper. A flexible concept means that if a target or multiple targets are to be detected, the FPMIMO radar system tries as much as possible to achieve the detection goal, including being able to minimize the impact of the clutter, the interference, and the other disturbances, by adjusting M and N, adapting the performance parameters to the desired target conditions. Accordingly, the radar can take the benefit of a programmable software-defined-radio (SDR) platform to meet specific requirements for various radar applications by exploiting the capability of SDR in performing the functions of devices used in conventional Tx and Rx, such as mixers, filters, and others, in the digital domain.

All the parameters of the SMIMO radar performance that have been mentioned are functions of M and N, which can be used to identify the possible combinations of M and N

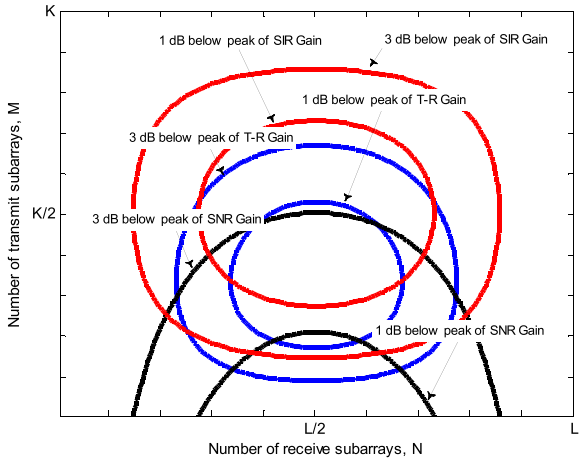

FIGURE 17. Combined contours of T-R, SNR, and SIR gains of FPMIMO radar for various combinations of number M of transmit subarrays versus number N of receive subarrays with equal number of antennas $K = L$ [31].

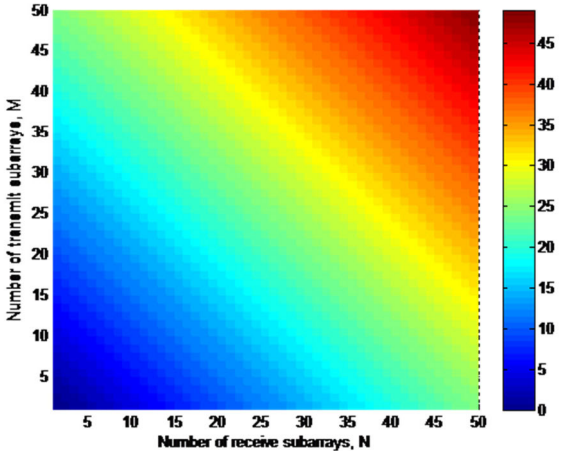

FIGURE 18. The maximum number of detectable targets (P_{max}) vs. the number of Tx-Rx subarrays (M and N) for FPMIMO radar with $K = L = 50$.

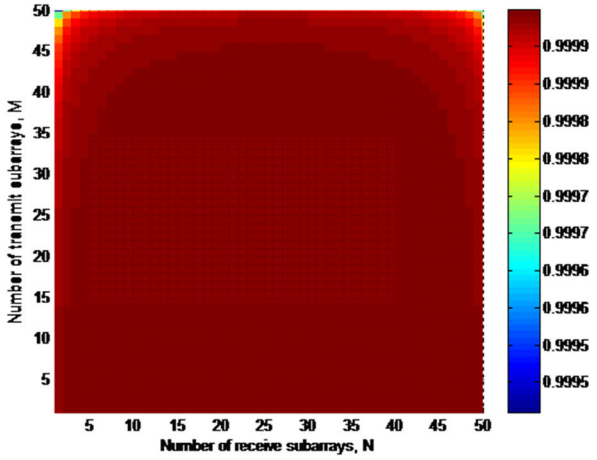

FIGURE 19. The probability of detection (P_d) vs. the number of Tx-Rx subarrays (M and N) for FPMIMO radar with $K = L = 50$, $V_T = 30$, $\sigma_p^2 = 1$, and $\sigma_n^2 = 0.1$.

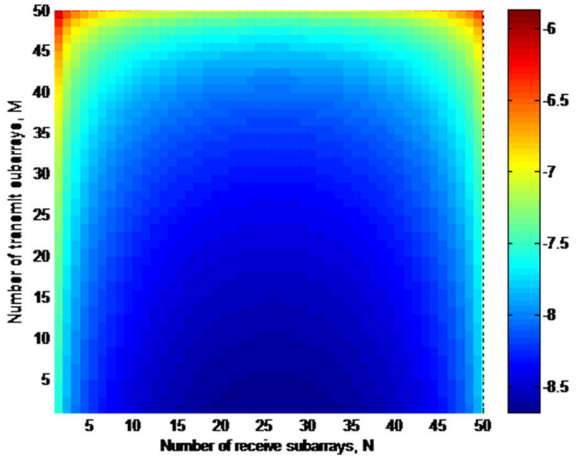

FIGURE 20. The probability of false alarm in logaritmic scale vs. the number of Tx-Rx subarrays (M and N) for FPMIMO radar with $K = L = 50$, $V_T = 30$, $\sigma_p^2 = 1$, and $\sigma_n^2 = 0.1$.

that provide the desired performance to detect multi-targets. Fig. 17, taken from [31, Fig. 3] with modified colouring for better clarity, presents a few examples of contour diagrams of the performance parameters, such as G_{TR}, SNR, and SIR as functions M and N.

The other advantages of the flexible SMIMO radar are the ability in governing the number of elements in VA and the maximum number of target detections by adjusting M and N. The VA is formed because Tx array transmits M orthogonal waveforms to form a more focused beampattern and echo signals are received by N Rx subarrays that act as independent elements. An example of the P_{max} diagram as a function of M and N for $K = L = 50$ is presented in Fig. 18, which agrees with the results in [13] and [17] that show that the characteristics of VA strongly determine P_{max}.

The performance of target detection presented on Figs. 19 and 20 are for the probability of detection and the probability of false alarm, respectively, as functions of M and N, where the effects of M and N have been reviewed in the explanation that follows Fig. 16. Fig. 20 depicts that the effect of M and N on the performance of P_{fa} is very closely related to the effect on the P_d, which is directly related to P_{fa}, as indicated by (78).

B. EXAMPLES OF APPLICATION

From the results in [31] and by evaluating various performance parameters in earlier sections of this paper, the SMIMO radar concept is ready for various radar applications. Examples of performance evaluation of the FPMIMO radar for the bird radar application have been presented in [31]. Another example of application is the vehicular radar, in which the relevant performance parameters are presented herein, such as P_{max}, $\mathcal{N}$, P_d, and P_{fa}.

A vehicular radar should be able to measure the range and the velocity of distant objects with sufficient precision compared to other types of sensor instruments, especially when the environmental conditions are not bright (i.e., foggy or dusty), because the radar is not affected by

TABLE 3. Mission requirement for vehicular radar.

Parameter	Symbol	Value
Min. SNR, dB	SNR_{min}	10
RCS, m^2	σ_p	1
Threshold value	V_T	32.8
Probability of false alarm	P_{fa}	$\geq 10^{-4}$

TABLE 4. Comparison of detection performance of FPMIMO radar with variants (*M*, *N*) pairs for vehicular radar application.

Parameter	PA (M=1,N=8)	MIMO (M=N=8)	PMIMO (M=4,N=8)	FPMIMO (M=N=4)
P_{max}	4	[7, 32]	[6, 20]	[3, 8]
$\mathcal{N}$	8	[15, 64]	[11, 32]	[7, 16]
P_{fa} (%)	0.0006	0.0047	0.0009	0.0004
P_d (%)	99.765	98.456	99.639	99.844

extreme environmental conditions such as heat, weather conditions, or variations of light or lighting on the road [35], [38].

The main concept of radar sensors utilized in vehicles has been reported by [36]. As the vehicular radar, the radar with high accuracy and resolution of multiple target detection is needed [38]. The challenge is that in addition to estimating the range, the velocity, and the azimuth angle of the target, the radar must also be able to achieve a sufficient maximum number of detectable targets and capability to decide on the presence or absence of the target (i.e., probability of detection) when used for multi-target detection. Therefore, it is necessary to formulate the mission requirements for the vehicular radar implementation, as given in Table 3.

This example aims to provide technical recommendations for adjusting the array parameters and implementing the FPMIMO system in vehicular radar applications as illustrated in Fig. 21. For vehicular radar applications, the radar system is illustrated as having a radar beam that covers a span of the azimuth angle.

In this example, the vehicular radar application adopts isotropic or omnidirectional antennas with the number of Tx and Rx antennas being $K = L = 8$ and the element spacing being half wavelength. The linear structure has an optimum subarray, which is $M = N = 4$. We subsequently obtain:

a. The range of P_{max} by applying (32), i.e. [3, 8].
b. The range of $\mathcal{N}$ from (16), i.e. [7, 16].
c. For P_{fa} of 10^{-6}, V_T of 32.8 is obtained [34].
d. Following [33] for $SNR_{min} \geq 10$ dB and $P_{fa} \geq 10^{-4}$ [33] and using (80), P_d of99.8% is obtained. This confirms that all radars in Fig. 17 exhibit good detection performance in P_d and P_{fa} for SNR $\geq$ 10 dB.

Performance of the FPMIMO vehicular radar with various configurations are summarized in Table 4. As can be seen, the FPMIMO radar when combined with the SDR technology has the potential benefit of flexibility in adjusting the number of subarrays in Tx and Rx based on the current target conditions in order to achieve the desired performance parameters.

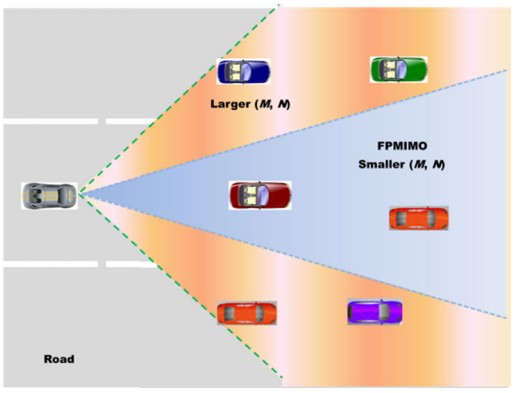

FIGURE 21. The FPMIMO radar application for vehicular radar.

VI. CONCLUSION

We have discussed the parameter identifiability of the FPMIMO radar and determined the maximum number of detected targets by the LS method. The maximum number of detectable targets is dictated by the number of virtual elements in a virtual array. To complete the discussion on the detection performance also given expression and evaluation of the probability of detection (P_d) and the probability of false alarm (P_{fa}). It has been shown that for a given total number of antennas at the transmit and receive sides, the parameter identifiability, the virtual array size, the probability of detection and of false alarm can be adjusted by varying the number of overlapping subarrays in the Tx-Rx arrays, which consequently varies the number of elements in each subarray. Expressions of the parameter identifiability, the magnitude of target reflection coefficient, the virtual array, the probability of detection, and the probability of false alarm for the general FPMIMO radar have been given, which all depend on the number of the Tx-Rx subarrays and which lead to some well-known radar forms as special cases, including the PA radar, the MIMO radar, and the PMIMO radar.

In this manner, the FPMIMO radar can achieve a desired magnitude of complex amplitude, again by adjusting the number of Tx-Rx subarrays, which essentially is equivalent to trading off between the waveform diversity gain and the directional coherent gain. This flexibility suits the FPMIMO radar for various applications having different requirements of parameter identifiability, the minimum magnitude of target reflection coefficient, the virtual array, the probability of detection, and the probability of false alarm. When implemented on a SDR platform, flexibility in the radar design can be achieved. Finally, a design example has been presented of the FPMIMO radar configuration for vehicular radar applications.

ACKNOWLEDGMENT

The authors are grateful to Prof. W. Bösch and Dr. H. Schreiber of Graz University of Technology, Austria for their kind assistance during the first author's sandwich program in Graz and feedbacks that greatly improved the manuscript.

REFERENCES

[1] R. C. Hansen, *Phased Array Antennas*, 2nd ed. Hoboken, NJ, USA: Wiley, 2009.

[2] D. S. Zrnic, G. Zhang, and R. J. Doviak, "Bias correction and Doppler measurement for polarimetric phased-array radar," *IEEE Trans. Geosci. Remote Sens.*, vol. 49, no. 2, pp. 843–853, Feb. 2011.

[3] S. J. Wijnholds and W. A. Van Cappellen, "*In situ* antenna performance evaluation of the LOFAR phased array radio telescope," *IEEE Trans. Antennas Propag.*, vol. 59, no. 6, pp. 1981–1989, Jun. 2011.

[4] I. Immoreev and T.-H. Tao, "UWB radar for patient monitoring," *IEEE Aerosp. Electron. Syst. Mag.*, vol. 23, no. 11, pp. 11–18, Nov. 2008.

[5] A. Leshem, J. Christou, B. D. Jeffs, E. Kuruoglu, and A. J. van der Veen, "Introduction to the issue on signal processing for space research and astronomy," *IEEE J. Sel. Topics Signal Process*, vol. 2, no. 5, pp. 609–612, Oct. 2008.

[6] J. Li, P. Stoica, and X. Zheng, "Signal synthesis and receiver design for MIMO radar imaging," *IEEE Trans. Signal Process.*, vol. 56, no. 8, pp. 3959–3968, Aug. 2008.

[7] I. Bekkerman and J. Tabrikian, "Target detection and localization using MIMO radars and sonars," *IEEE Trans. Signal Process.*, vol. 54, no. 10, pp. 3873–3883, Oct. 2006.

[8] W. Wang, "Applications of MIMO technique for aerospace remote sensing," in *Proc. IEEE Aerosp. Conf.*, Big Sky, MT, USA, Mar. 2007, pp. 1–10.

[9] A. Haimovich, R. Blum, and L. Cimini, "MIMO radar with widely separated antennas," *IEEE Signal Process. Mag.*, vol. 25, no. 1, pp. 116–129, Dec. 2008.

[10] Y. Li, H. Ma, Y. Wu, L. Cheng, and D. Yu, "DOA estimation for echo signals and experimental results in the AM radio-based passive radar," *IEEE Access*, vol. 6, pp. 73316–73327, 2018.

[11] A. Hassanien and S. A. Vorobyov, "Transmit/receive beamforming for MIMO radar with colocated antennas," in *Proc. IEEE Int. Conf. Acoust., Speech Signal Process.*, Taipei, Taiwan, Apr. 2009, pp. 2089–2092.

[12] D. Wilcox and M. Sellathurai, "On MIMO radar subarrayed transmit beamforming," *IEEE Trans. Signal Process.*, vol. 60, no. 4, pp. 2076–2081, Apr. 2012.

[13] J. Li, P. Stoica, L. Xu, and W. Roberts, "On parameter identifiability of MIMO radar," *IEEE Signal Process. Lett.*, vol. 14, no. 12, pp. 968–971, Dec. 2007.

[14] L. Xu, J. Li, and P. Stoica, "Target detection and parameter estimation for MIMO radar systems," *IEEE Trans. Aerosp. Electron. Syst.*, vol. 44, no. 3, pp. 927–939, Jul. 2008.

[15] T. D. Backes, "Parameter identifiability in a phased-subarray MIMO radar," in *Proc. IEEE Aerosp. Conf.*, Big Sky, MT, USA, Mar. 2014, pp. 1–6.

[16] X. Song, N. Zheng, and T. Bai, "Resource allocation schemes for multiple targets tracking in distributed MIMO radar systems," *Int. J. Antennas Propag.*, vol. 2017, Jul. 2017, Art. no. 7241281.

[17] M. Davis, G. Showman, and A. Lanterman, "Coherent MIMO radar: The phased array and orthogonal waveforms," *IEEE Aerosp. Electron. Syst. Mag.*, vol. 29, no. 8, pp. 76–91, Aug. 2014.

[18] Z. Qiu, X. Li, H. Chen, Z. Zhuang, and J. Yang, "Effects of transmitting correlated waveforms for co-located multi-input multi-output radar with target detection and localisation," *IET Signal Process.*, vol. 7, no. 9, pp. 897–910, Dec. 2013.

[19] C. Duofang, C. Baixiao, and Q. Guodong, "Angle estimation using ESPRIT in MIMO radar," *Electron. Lett.*, vol. 44, no. 12, p. 770, 2008.

[20] G. Oliveri and L. Poli, "Synthesis of monopulse sub-arrayed linear and planar array antennas with optimized sidelobes," *Prog. Electromagn. Res.*, vol. 99, pp. 109–129, 2009.

[21] D. Petrolati, P. Angeletti, and G. Toso, "A lossless beam-forming network for linear arrays based on overlapped sub-arrays," *IEEE Trans. Antennas Propag.*, vol. 62, no. 4, pp. 1769–1778, Apr. 2014.

[22] A. Hassanien and S. A. Vorobyov, "Phased-MIMO radar: A tradeoff between phased-array and MIMO radars," *IEEE Trans. Signal Process.*, vol. 58, no. 6, pp. 3137–3151, Jun. 2010.

[23] A. Roshanzamir and M. Bastani, "Hybrid orthogonal-phased array MIMO RADAR," in *Proc. IET Int. Radar Conf.*, 2013, pp. 1–5.

[24] W.-Q. Wang, "Phased-MIMO radar with frequency diversity for range-dependent beamforming," *IEEE Sensors J.*, vol. 13, no. 4, pp. 1320–1328, Apr. 2013.

[25] W. Khan, I. M. Qureshi, A. Basit, and M. Zubair, "Hybrid phased MIMO radar with unequal subarrays," *IEEE Antennas Wireless Propag. Lett.*, vol. 14, pp. 1702–1705, 2015.

[26] W. Khan, I. M. Qureshi, and K. Sultan, "Ambiguity function of phased–MIMO radar with colocated antennas and its properties," *IEEE Geosci. Remote Sens. Lett.*, vol. 11, no. 7, pp. 1220–1224, Jul. 2014.

[27] S. Tahcfulloh and G. Hendrantoro, "Phased-MIMO radar using Hadamard coded signal," in *Proc. Int. Conf. Radar, Antenna, Microw., Electron., Telecommun. (ICRAMET)*, Tangerang, Indonesia, Oct. 2016, pp. 13–16.

[28] A. Alieldin, Y. Huang, and W. M. Saad, "Optimum partitioning of a phased-MIMO radar array antenna," *IEEE Antennas Wireless Propag. Lett.*, vol. 16, pp. 2287–2290, 2017.

[29] S. Tahcfulloh and G. Hendrantoro, "Phased MIMO radar with coherent receive arrays," in *Proc. Int. Conf. Signals Syst. (ICSigSys)*, Bali, Indonesia, May 2017, pp. 72–76.

[30] M. Hardiwansyah, S. Tahcfulloh, and G. Hendrantoro, "Parameter identifiability of phased-MIMO radar," in *Proc. Int. Conf. Artif. Intell. Inf. Technol. (ICAIIT)*, Yogyakarta, Indonesia, Mar. 2019, pp. 192–195.

[31] S. Tahcfulloh and G. Hendrantoro, "Full phased MIMO radar with colocated antennas," *Int. J. Commun. Antenna Propag.*, vol. 9, no. 2, p. 144, Jul. 2019.

[32] E. Fishler, A. Haimovich, R. Blum, L. Cimini, D. Chizhik, and R. Valenzuela, "Spatial diversity in radars–models and detection performance," *IEEE Trans. Signal Process.*, vol. 54, no. 3, pp. 823–838, Mar. 2006.

[33] M. I. Skolnik, *Introduction to Radar Systems*, 3rd ed. New York, NY, USA: McGraw-Hill, 2002.

[34] H. Meikle, *Modern Radar Systems*, 2nd ed. Boston, MA, USA: Artech House, 2008.

[35] R. H. Rasshofer and K. Gresser, "Automotive radar and Lidar systems for next generation driver assistance functions," *Adv. Radio Sci.*, vol. 3, pp. 205–209, Apr. 2010.

[36] E. Lissel, H. Rohling, and W. Plagge, "Radar sensor for car applications," in *Proc. IEEE Veh. Technol. Conf. (VTC)*, Dec. 2002, pp. 438–442.

[37] B. R. Mahafza, *Radar Signal Analysis and Processing Using MATLAB*. Boca Raton, FL, USA: Chapman-Hall, 2009.

[38] I. Bilik, O. Longman, S. Villeval, and J. Tabrikian, "The rise of radar for autonomous vehicles: Signal processing solutions and future research directions," *IEEE Signal Process. Mag.*, vol. 36, no. 5, pp. 20–31, Sep. 2019.

SYAHFRIZAL TAHCFULLOH received the B.Eng. degree in electrical engineering from Universitas Gadjah Mada, Yogyakarta, Indonesia, in 2003, and the M.Eng. degree in electrical engineering from the Institut Teknologi Sepuluh Nopember (ITS), Surabaya, Indonesia, in 2010. He has been a Lecturer with Universitas Borneo Tarakan, Tarakan, Indonesia, since 2004, and has been on leave from work to pursue the Ph.D. degree with the Institut Teknologi Sepuluh Nopember, since 2015. His research interests include array signal processing and MIMO radars.

GAMANTYO HENDRANTORO (Senior Member, IEEE) was born in Jombang, Indonesia, in November 1970. He received the B.Eng. degree in electrical engineering from the Institut Teknologi Sepuluh Nopember (ITS), Surabaya, Indonesia, in 1992, and the M.Eng. and Ph.D. degrees in electrical engineering from Carleton University, Ottawa, Canada, in 1997 and 2001, respectively. He has been involved in various collaborative studies, including the investigation of millimeter-wave propagation and wireless systems for tropical areas, studies on HF skywave channels and communications in equatorial regions, and the development of radar array and signal processing. He is currently a Professor with the Department of Electrical Engineering, ITS. His research interests include radio propagation channel modeling, wireless communications, array signal processing for communications, and radar systems. He was ranked third at the 2005 National Selection of University Lecturers with Best Achievement by the Indonesian Ministry of Education. He has received a number of awards, including the URSI Young Scientist Award, in 2005, and the ITS Laboratory-Based Education Award, in 2014.